CHALMERS
UNIVERSITY OF TECHNOLOGY

Development of methods to understand the dynamics of lung delivered mRNA

Master's thesis in Biomedical engineering

KOPIKA KUGATHASAN

Department of Chemistry and Chemical Engineering
CHALMERS UNIVERSITY OF TECHNOLOGY
Gothenburg, Sweden 2020

Master's thesis 2020:KBTX12

Development of methods to understand the dynamics of lung delivered mRNA

KOPIKA KUGATHASAN

CHALMERS
UNIVERSITY OF TECHNOLOGY

Chemistry and Chemical Engineering
Division of Chemistry and Biochemistry
Wilhelmsson Research Group
Chalmers University of Technology
Gothenburg, Sweden 2020

Development of methods to understand the dynamics of lung delivered mRNA
KOPIKA KUGATHASAN

Supervisor: Karin Björhall, Bioscience COPD/IPF,
BioPharmaceuticals R&D, Research and Early Development,
Respiratory & Immunology, AstraZeneca R&D Gothenburg

Examiner: Marcus Wilhelmsson, Chemistry and Chemical Engineering,
Chalmers university of technology

Master's Thesis 2020:KBTX12
Chemistry and Chemical Engineering
Division of Chemistry and Biochemistry
Wilhelmsson Research Group
Chalmers University of Technology
SE-412 96 Gothenburg
Telephone +46 31 772 1000

Typeset in LaTeX
Printed by Chalmers University of Technology.
Gothenburg, Sweden 2020

Development of methods to understand the dynamics of lung delivered mRNA
KOPIKA KUGATHASAN
Chemistry and Chemical Engineering
Chalmers University of Technology

Abstract

Chronic Obstructive Pulmonary Disease (COPD) is a global burden that currently lacks good treatments to reverse the disease progression. Messenger ribonucleic acid mRNA together with nano carriers like lipid nanoparticles (LNPs) holds a broad potential as future treatments for a wide range of diseases, including respiratory diseases like COPD. In this project, methods to monitor protein translation after mRNA treatments were developed. In mouse lung dissociation experiments to obtain a single cell suspension, this thesis shows that endotracheal delivery of the protease dispase at the time of tissue harvest was of great advantage to maximize harvest of epithelial cells, identified as EpCAM+ (CD326+) cells in flow cytometry. The developed method can in the future be incorporated into inhalation drug research when testing different mRNA:LNP combinations *in vivo* to validate the recipient cell populations.
This master thesis also involved development of *in vitro* methods for detection of protein translation after mRNA delivery. For this purpose, LA-4 cells, a murine epithelial cell line, was transfected with enhanced green fluorescent protein (eGFP) mRNA formulated with Lipofectamine MessengerMax, a commercially available mRNA transfection reagent, and the protein expression was monitored over time. In addition, an initial experiment to explore eGFP mRNA:Lipofectamine MessengerMax transfection of human lung explants was performed. In conclusion, these methods can be used for characterization of resulting protein expression after *in vitr*o and *in vivo* delivery of different LNPs and mRNAs.

Keywords: COPD, Mouse lung dissociation, mRNA, Lipid nanoparticle, Enhanced green fluorescent protein, cell transfection, Tissue transfection, Alveolar epithelial cells, Flow cytometry, Cell real-time imaging

Acknowledgements

This project is performed at AstraZeneca, R&D, Mölndal and supervised by Karin Björhall. I would like to express my sincere thanks to my supervisor, guide, teacher and friend, Karin Björhall, who has been so kind to assist me with the experiments and report writing.
I am grateful to my examiner, Marcus Wilhelmsson, for being generous with guidance and feedback on my work.
I would also like to extend my gratitude to the former program director of MPBME program, Ants Silberberg, to encourage me to pursue this thesis from the beginning until the content was altered due to COVID-19 outbreak lock-down.

Last, but not the least, my parents, relatives and dear friends deserve my heartfelt thanks and love too.

Kopika Kugathasan, Gothenburg, June 2020

Contents

Acronyms

AAT α_1-antitrypsin. 8, 9
AT-I Alveolar type I. 6, 8, 34, 36
AT-II Alveolar type II. 6–8, 34–36

CF Cystic Fibrosis. 3
COPD Chronic Obstructive Pulmonary Disease. v, 1–3, 8, 9

DNA Deoxyribonucleic acid. 13
DNAse Deoxyribonuclease. 13, 18

eGFP Enhanced green fluorescence protein. v, ix, x, VI, 4, 13, 16, 23–27, 38–43
ELISA Enzyme-linked immunosorbent assay. 26
endo-EVs Extracellular vesicles of endosomal origin. 12

FBS Fetal bovine serum. 19, 21, 23
FMO Fluorescence Minus One. ix, 15
FSC Forward scattered light. 13–15

GOLD Global initiative for chronic obstructive lung disease. 1, 8

i.t intratracheal. 4

LNP Lipid nanoparticle. v, 2, 4, 11, 12, 16

MFI Median fluorescence intensity. 25, 40
MHC-II Major histocompatibility complex class II. 7
mRNA Messenger ribonucleic acid. v, ix, x, VI, 1–4, 9–13, 16, 23, 24, 26, 27, 38–43
mRNA:LNP mRNA encapsulated with LNP. ix, 2–4, 9, 10, 12, 17, 26, 43

NEAA Non-essential amino acids. 23

PBS Phosphate buffered saline. I, II, 17–19, 21, 23, 26
PD Pharmacodynamics. 4
PK Pharmacokinetics. 4

RBC Red blood cell. 7, 31
RNAse Ribonuclease. 2, 10, 11
RT Room temperature. 19, 25
RV Residual Volume. 9

SSC Side scattered light. 14, 15

STD Standard deviation. 35, 37

TLR Toll-like receptors. 7, 11

UTR Untranslated region. 10

WHO World Health Organization. 1

1
Introduction

1.1 Background

In the long list of lung diseases, Chronic Obstructive Pulmonary Disease (COPD) holds a top place. COPD is defined by irreversible air flow obstruction associated with inflammatory response in the small airways of the lung against inhaled harmful particles in the air. The inflammatory response of COPD is mainly attributed to causes that vary across countries. Long-term exposure of tobacco is a main agent in the western countries, whereas toxic gases, out- and in-house smokes are more common causes in the developing countries.[1]

Classically, the multifactorial disease COPD includes two different morphological forms; chronic bronchitis and emphysema.[2] Chronic bronchitis is characterized by cough due to hypersecretion of mucus, that does not necessarily result in airway obstruction. Emphysema is defined by parenchymal tissue destruction and a permanent airspace enlargement. These two types of airway obstructions are clearly visualized in Figure 1.1.[3]

In terms of the global prevalence, there were 251 million cases of COPD reported in 2016 and 3.17 million deaths in 2015. This represents 5% of all deaths globally in 2015, according to World Health Organization (WHO).[4] Because of the increasing incidence of COPD, WHO formed the Global initiative for chronic obstructive lung disease (GOLD) in 1997, composed of a team of health care professionals around the world that works to raise awareness and improve treatment and prevention of COPD.[5]

A cure against COPD that would significantly improve the lung function is yet to be discovered and the current treatment options, beyond lung transplantation, are aimed to merely tame the difficulty in breathing or to relieve symptoms. Therefore, there is a great need for a new drug that targets the molecular mechanisms of COPD.[6]

Messenger ribonucleic acid (mRNA) engineering has recently emerged as a potential modality in the field of drug delivery. When mRNA is used as a drug, it can be utilized in a wide range of applications such as protein supplementation and for vaccination purposes. A great advantage of RNA, as opposed to DNA, is that RNA does not need to pass the nuclear membrane or manipulate the genome permanently for the desired protein to be transcribed, which facilitates instant response. Moreover, the biodegradability and transient nature of mRNA potentially reduces the risk of adverse effects. However, in order to incorporate mRNA in therapeutic platforms, several hurdles need to be overcome.

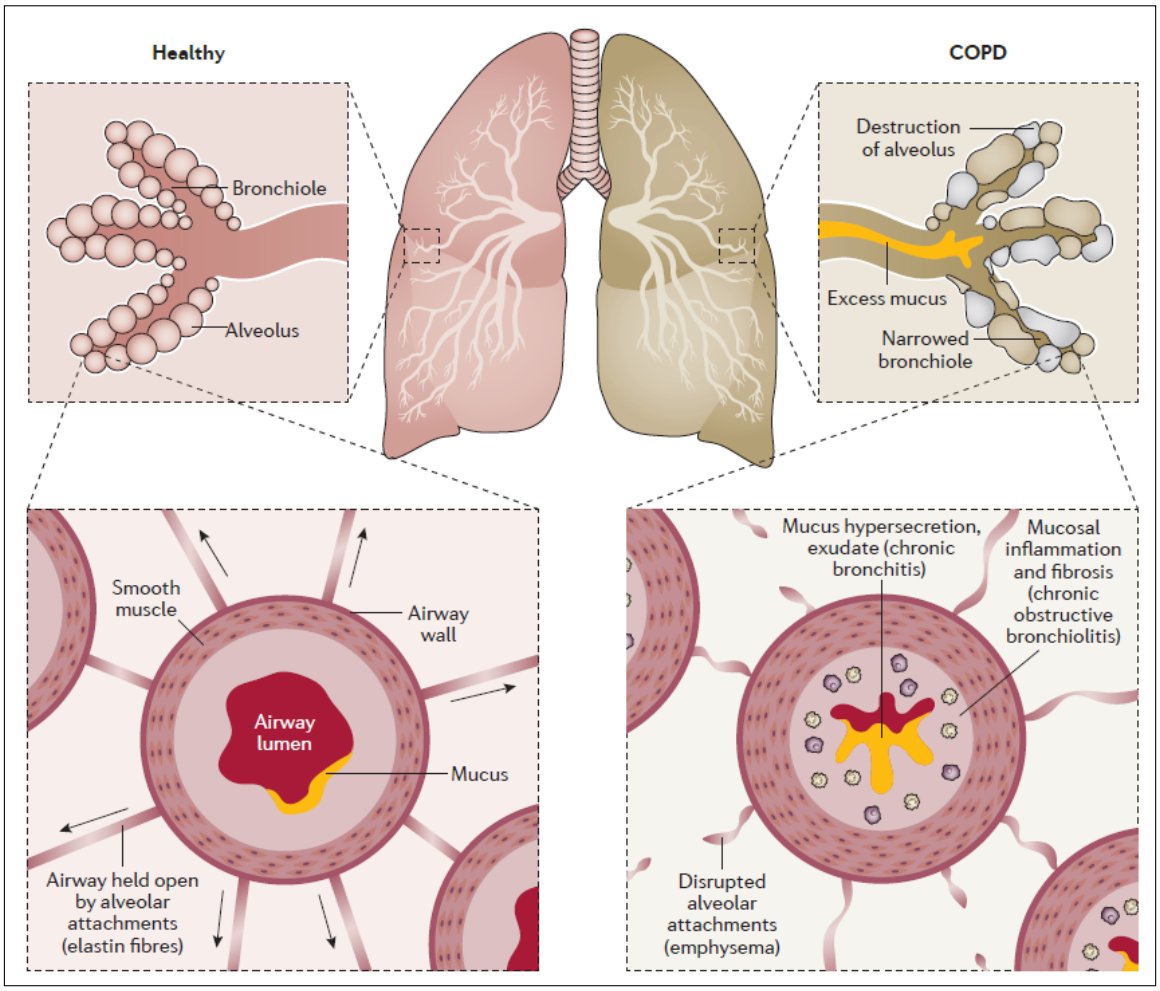

Figure 1.1: The small airways of a healthy lung are open with less mucus and the alveolar walls supported by elastin fibers. In a COPD lung, the small airways are narrowed by thickening of the peripheral walls, there is hypersecretion of mucus and disruption of alveolar attachments to the elastin fibers.[7]

Wildtype mRNA, which is less stable than DNA, can be modified to give prolonged stability, low immunogenicity and improved capacity of protein translation.[8][9] Another aspect to be explored in the mRNA therapeutic field is a delivery modality to enable delivery of mRNA into the cells. The carrier can facilitate the crossing of the negatively charged mRNA across the plasma membrane, reduce immunogenicity and protect the mRNA from ribonuclease (RNAse) degradation. Chemically modified nanocarriers such as lipid nanoparticle (LNP) have been a recent breakthrough in the field of mRNA delivery. LNPs can facilitate cell internalization and gradual endosomal release of mRNA in the cytoplasm of the cell in order to provide optimal protein translation. Kinetics of mRNA encapsulated with LNP (mRNA:LNP) transfection is presented in Figure 1.2.[10][11]
Several mRNA:LNP therapeutics are under development in the field of respiratory diseases, for example CFTR mRNA as a protein supplementation strategy to treat

Cystic Fibrosis (CF) and most recently stabilized spike (S) protein mRNA (mRNA-1273) as a intravenously delivered vaccine against COVID-19.[12][13] Translate Bio, a clinical pharmaceutical company focusing on development of mRNA therapeutics to treat pulmonary diseases, is currently in Phase I/II clinical trials with MRT5005, a mRNA:LNP therapy aiming at restoring the function of the disease-causing ion channel protein CFTR in CF by protein supplementation of non-mutated CFTR. The MRT5005 represents the first of mRNA:LNP in clinical phase that targets the lung specifically and is delivered by nebulisation.[12]
In the spectrum of COPD, α_1-antitrypsin deficiency (AATD) contribute to emphysema. α_1-antitrypsin, also known as SERPINA1, is a protein responsible for the protease and anti-protease homeostasis in the lung. AATD, caused by mutations within *SERPINA1* gene, has successfully been proven to be treated efficiently with *SERPINA1* mRNA encapsulated with liposomal nanoparticle *in vitro* and *in vivo*.[14]
AstraZeneca is currently in a collaboration with Ethris GmbH, a leader in mRNA-based therapeutics for the development of new stabilised non-immunogenic modified RNA therapies, named SNIM®RNA technology, for respiratory diseases. The collaboration focuses on developing mRNA therapeutics for respiratory diseases, for example COPD.[15]

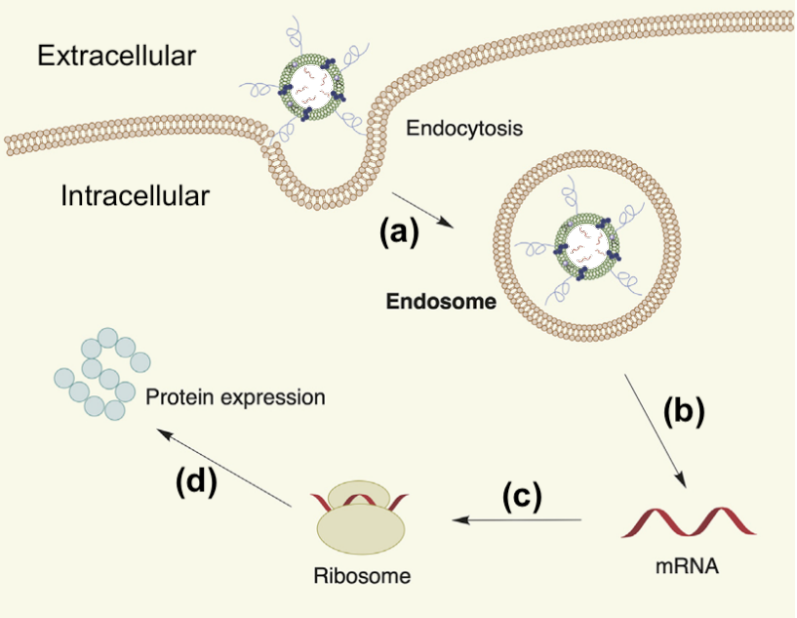

Figure 1.2: Lipid nanoparticle-based mRNA delivery: (a) cellular transfection of mRNA:LNP into endosome, (b) release of mRNA into the cytoplasm (c) translation of mRNA and (d) protein expression.[8]

1.2 Aim

The primary aim of this project was to develop and optimize a protocol for mouse lung dissociation and characterize the cells based on the different cell markers of lung

tissue. The optimized protocol will be used to detect downstream protein expression after *in vivo* intratracheal (i.t) or nebulized delivery of mRNA:LNP to elucidate which cell types have received the mRNA:LNP and express the intended protein. The developed methods could also be used in isolating primary cell types out of the lung for further *in vitro* studies. The optimization was targeted to generate maximal number of epithelial cells in the single cell suspension, since inhalation therapy of mRNA is firstly encountered by epithelial cells and is the target cell type for many inhaled therapies.
Another goal of this project was to understand the dynamics of lung delivered mRNA by studying the transfection and protein expression rates of enhanced green fluorescence protein (eGFP) *in vitro*. The experiments were carried out by using lipofectamine MessengerMAX as a carrier, since lipofectamine MessengerMax has been proven to give high efficiency in delivering mRNA. [16] The results from this experiment would later be utilized by inhaled mRNA drug projects to investigate the pharmacokinetics (PK) and pharmacodynamics (PD) of mRNA:LNP delivery into the lung *in vitro* and *in vivo*, where PK is defined by how an organism affects a drug and how the drug affects the organism is given by PD.[17]

1.3 Limitations

To understand the dynamics of mRNA delivery to the lung, a murine epithelial cell line was targeted with the mRNA sequence of eGFP. The readout of this set of experiments was measurements of fluorescent protein expression, wheras mRNA uptake in the cells were not measured. Although, the final goal of the RNA therapies in AstraZeneca is to design LNPs as drug carriers, tests on LNPs was not performed in this study. Instead, Lipofectamine MessengerMax was used in the experiments as a model to mimic the dynamics of LNPs.

1.4 Ethical approvals

Mouse lung samples
For the lung dissociation experiments, mouse lungs were obtained from the animal house at AstraZeneca and the present study was approved by the local Ethical committee in Gothenburg and the number of approval is EA: 002131-2019.
Human lung samples
For the mRNA delivery experiments, human lung tissue samples were acquired from the Department of Cardiothoracic Surgery at Sahlgrenska University Hospital in Gothenburg. The study was approved by the Swedish Research Ethical Committee in Gothenburg (1026-15). Study and consent procedures were reviewed and approved by the Swedish Research Ethical Committee in Gothenburg, Sweden (FEK 675-12/2012 and 1026-15, March 2016) in accordance with principles of the Declaration of Helsinki. Written informed consent was obtained preoperatively.

2

Theory

2.1 Anatomy and physiology of the human lung

The primary function of the respiratory system is to inhale O_2, a fuel for the cells to function and exhale CO_2, a waste product of the cell functions. The system is divided into two parts, upper and lower divisions of the respiratory tract. Upper division consists of the nose and pharynx, whereas the lower includes larynx, trachea, right and left bronchi and lung lobes, which is shown in Figure 2.1. The lower respiratory system is further divided into two functional and structural components: the conducting zone and respiratory zone. The conducting zone consists of trachea, bronchi and terminal bronchioles. The respiratory zone, as shown in Figure 2.2, is made up of the lung parenchyma that includes respiratory bronchioles, alveolar ducts, alveolar sacs and alveoli.[18]

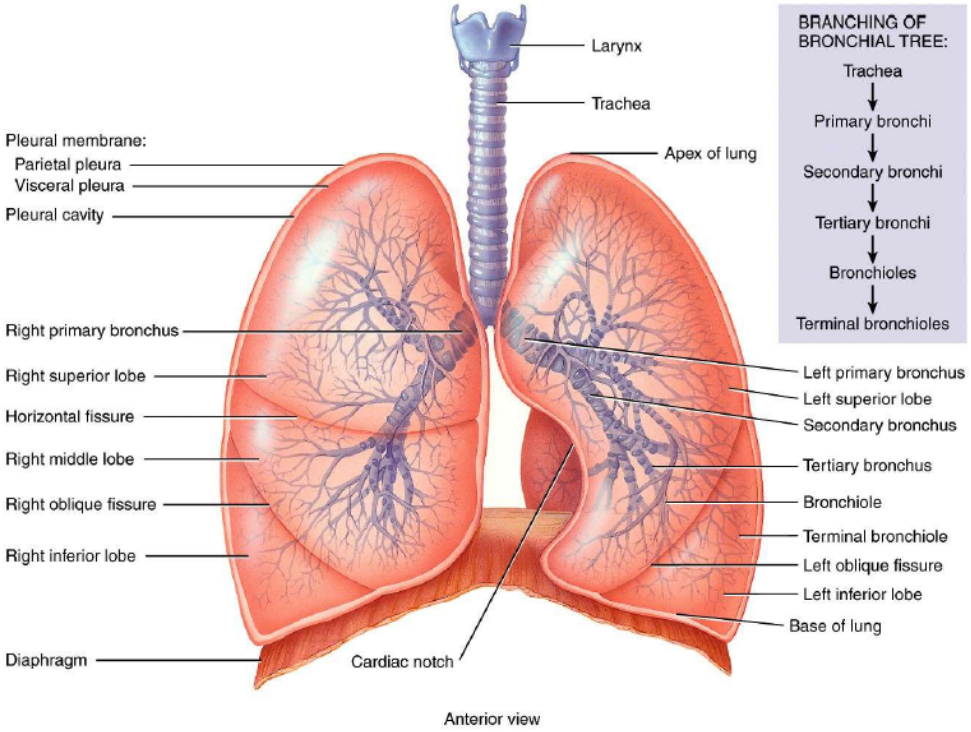

Figure 2.1: The components of lower division of the human respiratory tract.[18]

The bronchial tree comprises mainly of primary bronchus for each lung, secondary bronchus for each lung lobe and tertiary or segmented bronchus for each segments.

The cartilage and smooth muscle surrounding the bronchi provide mechanical structures that prevent the lung from collapsing and also assist in contraction/dilation of the lung.[19] Nasal cavity, trachea, bronchi and bronchioles are lined by pseudostratified columnar epithelial tissue, which is ciliated and the cilia assist in removing the particles that are trapped in respiratory mucus. Segmented bronchus includes bronchioles with no cartilage; conducting bronchiole, terminal bronchiole and respiratory bronchiole which is part of the respiratory zone.[18] There are approximately 300 million alveoli in the two adult human lungs which provide a surface area of at least $160m^2$ for gas exchange.[20]

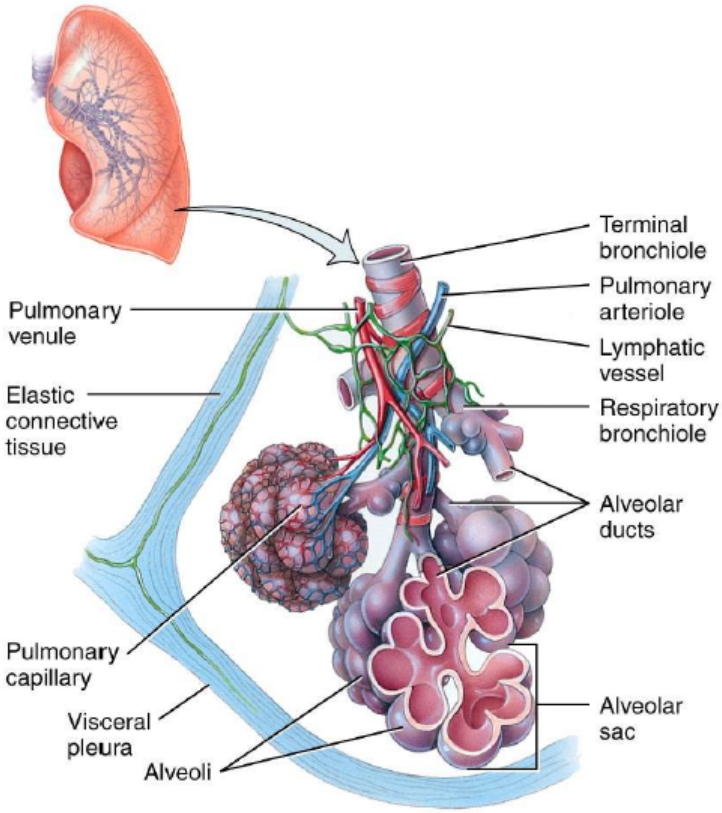

Figure 2.2: Terminal branchiole of a human lung that contains respiratory bronchiole which open at alveolar ducts that are made up of alveoli.[18]

Inspired air is conditioned and humidified, warmed and filtered as it travels through airway tubes and reaches the bronchioles. The air travels towards the alveolus and diffusion of CO_2 and O_2 occurs across the respiratory membrane, as shown in Figure 2.3(b). The alveoli contain type I and II alveolar epithelial cells and alveolar macrophages, see Figure 2.3(a). Alveolar type I (AT-I) cells of the alveolar compartment are terminally differentiated cells with a lifespan of about 120 days. AT-I cells are large, elongated and flattened, whereas alveolar type II (AT-II) cells are cuboidal secretory cells. As AT-I cells govern the gas exchange and constantly undergo excessive physical and chemical stresses, they require regular repair. AT-II cells are responsible for maintaining the alveolar homeostasis. They can proliferate and differentiate into AT-I cells and repair the damage, as they have

a progenitor function even under non-stressed conditions. Besides, AT-II cells secrete pulmonary surfactant into the alveolar space. The surfactant, composed of phospholipids and lipoproteins, reduce the surface tension at the air/liquid interface in the lung. Macrophages are also important cells of the alveoli responsible for the cleaning process in which they engulf apoptotic cells and foreign particles from the inhaled air.[18][21][22]

Pulmonary capillaries surround the alveolar sacs and the respiratory membrane is only 0.5 μm in wide. The alveolar sacs are also coated by fibroblasts and myofibroblasts that produce elastin and collagen fiber networks, that assist the respiration in inflating and deflating. The ability of the lung to rebound after having been inflated by inhalation is called elastic recoil. This phenomenon is maintained by elastin and elastic fibers in the connective tissue of the lungs to a high degree as well as the surface tension generated by surfactants secreted by AT-II cells.[1][18]

Pulmonary gas exchange is the diffusion of O_2 and CO_2 between the air to the blood, see Figure 2.3(b). Together with the partial pressure of the gases that facilitate the diffusion, the available total surface area of the respiratory membrane is an important factor for the rate of gas exchange. Diffused O_2 binds to the heme group that contains four ions of iron of deoxyhemoglobin, a protein in red blood cell (RBC) and is transported by the blood to the tissues. Hemoglobin also carries the body's CO_2 back to the respiratory membrane, but is bound to the amino groups of the protein and thus do not compete with oxygen for binding.[18]

2.2 Inflammatory response in the lung

The human immune system holds a critical task in the lung of repulsing invaders and orchestrating the repair of injury. The immune system consists of two main responses; innate and adaptive. The innate immune defense includes the non-specific identification and resistance to pathogens, for example tight junctions between the epithelial cells, pattern recognition receptors like toll-like receptors (TLR) on epithelial barriers, macrophages and the alveolar fluid and its surfactant proteins (SP-A and SP-D), secreted by AT-II cells. Second line of defense includes activation of cytokines by damaged epithelial cells and activated macrophages which can then lead to recruitment of additional immune cells from the blood, for example influx of neutrophils. Elastase is a protease class enzyme secreted by neutrophils that digests almost all extracellular matrix including elastin an elastic-fibers.[2][23]

Lung dendritic cells, a type of antigen presenting cells, engulf pathogens and present them in as epitopes on the major histocompatibility complex class II (MHC-II) that activates the adaptive immune system by promoting T helper cells, cytotoxic T cells and B lymphocytes. Although the immune response is critical to protect the lung from harmful pathogens, inappropriate responses can result in chronic lung diseases. The actions of immune defense can then lead to multiple issues in breathing, such as increased resistance of lung tissue due to fibrosis and smooth muscle tissue remodeling of the lung, thickening of airway walls due to mucus overproduction and the loss of ciliary function, ultimately resulting in airflow obstruction.[24][25]

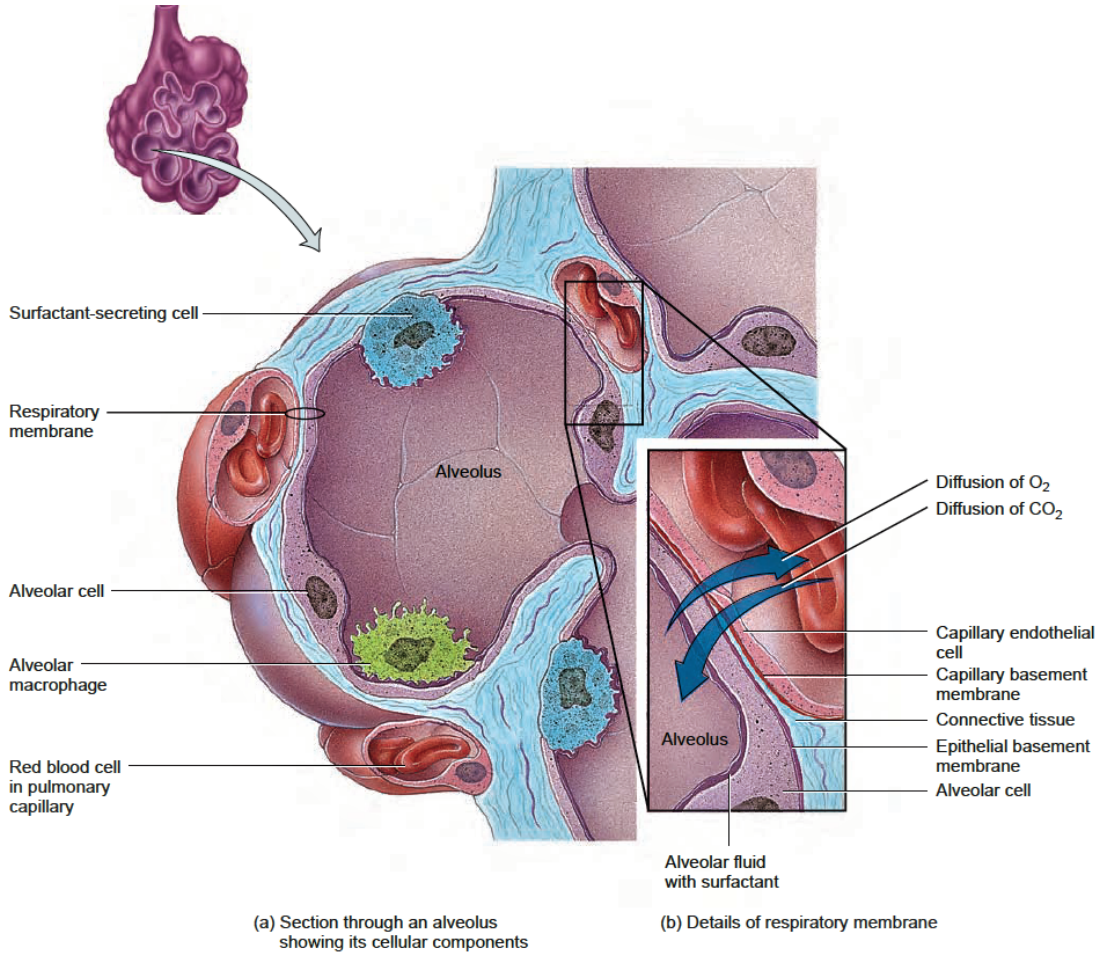

Figure 2.3: Alveolar lining of a human lung with magnified membrane structure: (a) Alveolar cell (AT-I), Surfacttant secreting cell (AT-II) and alveolar macrophage are part of an alveolus. (b) Pulmonary gas exchange, where both O_2 and CO_2 diffuse through the capillary basement membrane.[18]

2.3 COPD and its pathophysiology

COPD is characterized by poor air flow or air trapping. According to the guidelines of GOLD, the umbrella term COPD is defined as "a preventable and treatable disease with some significant extra pulmonary effects that may contribute to severity in individual patients. [...] The airflow limitation is usually progressive and associated with an abnormal inflammatory response of the lung to noxious particles of gases".[1] The pathogenic mechanisms of COPD are diverse. Generally, an enhanced or abnormal inflammatory response of the lung tissues to the inhaled foreign particles is the main mechanism of the disease. Activated neutrophils and macrophages induce the production of elastases which is hard to be counteracted by the antiproteases, such as α_1-antitrypsin (AAT), a native anti-protease, and this leads to a destructive lung that loses elastic recoil. Oxidative stress, resulting from an imbalance between oxidants and antioxidants, leads to apoptosis or necrosis for the exposed cells by neutrophils and neutrophilia. The oxidative stress can also disrupt the tight

junctions between adjacent epithelial cells that provide epithelial barrier function to the inhaled pathogens and increase permeability or leakage over the barrier, which may also play a critical role in the pathogenesis of COPD.[26] Oxidation of the catalytic site of AAT contributes to α_1-antitrypsin deficiency, which in turn leads to emphysema.[23] Inherited mutations in the AAT gene is also the most prominent genetic factors that predispose individuals to COPD.[7] The main phagocytic ability of alveolar macrophages to engulf apoptotic bodies is referred to as efferocytosis. Impaired efferocytosis may also lead to necrotic processes, which is another pathology of COPD. Autoimmune mechanisms and accelerated aging have also been discussed to be potential pathogenesis of COPD.[26] The adaptive immune system activated by the lung dendritic cells has been observed to increase the disease severity of COPD.[25]
In a COPD patient, the obstruction of the airflow causes alveolar hypoventilation, which contributes further to hypoxemia and hypercapnia. Hypoxia is characterized by inadequate oxygenation of the blood and hypercapnia is an excess of carbon dioxide in the blood. Air flow limitation of COPD, as studied, is both reversible and irreversible. Irreversible limitation is due to the loss of static elastic recoil which leads to an increase in the volume of lung. An increase in the residual volume (RV), the volume of air remaining in the lungs after a maximal exhalation, may lead to relatively mild airway diseases, whereas the increase in total lung capacity, that includes RV and the volume of air breathed out after deepest inhalation, is usually an indication of more severe long-standing lung disease like COPD.[1]

2.4 Therapeutic approaches in COPD

Smoking cessation is proven to reduce exacerbations of COPD. Current pharmacological treatments for COPD essentially provide temporary relief of symptoms. Bronchodilators, standard treatment for COPD currently on the market, are substances that act on receptors of postganglionic nerves, responsible for bronchoconstriction. Long acting- or short acting β_2-agonist (LABA or SABA) which acts on β_2-adrenergic receptor and long acting- or short acting- muscarinic antagonist (LAMA or SAMA), that acts on muscarinic receptor dilate the smooth muscles in the small airways. This treatment reduce breathlessness and improve health status of the COPD patient. Moreover, inhaled corticosteroids (ICS) decrease the inflammation and thereby improve the lung function, but long-term administrations of ICS can cause side effects.[6][7]

2.5 mRNA:LNP therapeutics for COPD

Development of mRNA therapeutics for different respiratory diseases hold great potential. Depending on the disease, different lung cells can be targeted such as epithelial cells, alveolar cells, immune cells (lung macrophages), stem cells etc. By choosing inhalation as route of delivery, the risk of systemic side effects is minimized. However there are several obstacles to overcome for the inhaled therapeutic mRNA. The mRNA has to:

- withstand shear forces during nebulization/inhalation.
- penetrate the mucus layer/liquid layer in the airways/alveoli.
- avoid triggering an immune response and being cleared by immune defense.
- enter the cells.
- escape the endosomes.
- be translated into the desired protein.

All these steps require careful design of both the mRNA and its carrier.[27]

2.5.1 Lung specific considerations for mRNA delivery by inhalation

Extracellular mucus and alveolar fluids presents major challenges when it comes to lung delivery. This physical barrier is a dominant defense mechanism developed to protect itself against inhaled substances, including pathogens. The respiratory mucus that lays on the tip of cilia of the epithelial cells has a critical role in clearance of foreign material. However, both the mucus and the mucociliary clearance is often impaired in lung disease. For example in CF, an autosomal recessive disorder caused by mutations in the *CFTR* gene, the presence of a persistent mucus which is much thicker than in a healthy lung has been proven difficult for the mRNA delivery.[27] COPD patients also often suffer from mucos hypersecretions. The content of mucus from a COPD patients is likely to change its physical and chemical properties as well as its viscoelasticity. The alveolar epithelium is, as mentioned, covered with fluid consisting of surfactant proteins and phospholipids with a main function of reducing the surface tension[18], but surfactant proteins like SP-A and SP-D also play an essential role in the pulmonary immune defense by opsonizing inhaled pathogens that are then eliminated by macrophages. The alveolar fluid therefore represents a immunological barrier that needs to be overcome in mRNA:LNP lung delivery.[27]

2.5.2 Design of mRNA

In order to synthesize therapeutic mRNA, several aspects of the structure and sequence of mRNA should be explored. Wild type mRNA is short-lived and is modified shortly after transcription. A matured mRNA with its different parts is presented in Figure 2.4. In order to mimic the native environment, a synthetic mRNA should undergo processes such as $5'$ Capping and modifications in $5'$ and $3'$ untranslated region (UTR) and codons. $5'$ Cap is required for ribosome binding of the mRNA for the translation, UTRs are involved in protein binding during translation. The poly(A) tail in the $3'$ end of the molecule is important for the stability of mRNA and efficient translation. Changes in $5'$ and $3'$ UTRs of the mRNA can improve recruitment of RNA-binding proteins and microRNAs in order to maximize the translational efficiency. Modifications in the $5'$ mRNA cap can improve resistance to decapping and RNAse degradation. Codon optimisation towards frequently used codons can also be used to improve protein translation.[10][28][29]

Figure 2.4: Structural components of a mature mRNA.[10]

2.5.3 Design of lipid nanoparticles

Delivery of mRNA is more challenging than small oligonucleotides because of its larger size. mRNA molecules are highly negatively charged, and this causes a major barrier when it comes to intracellular delivery that requires crossing of the cell's lipid bilayer membrane. To protect the mRNA from RNAse degradation and enable its crossing over the cellular membrane, different types of delivery methods have been developed, one of them being mRNA coformulation into lipid nanoparticles (LNPs). The LNPs form colloidal nanoparticle structures encapsulating the mRNA. They are designed not to trigger the immune response, facilitating the fusion with the cell membrane as well as the endosomal escape process and to be degradable. Their specific design can also be used to enable/promote specific uptake into specific organs and cells. Materials used to build the LNPs are ionizable/cationic lipids, polymers, dendrimers and cell penetration peptides (eg TLR antagonist).[8] An example of multicomponent LNP is presented in Figure 2.5. The ionizable behavior of cationic lipids have been shown to enhance endosomal escape and facilitate the cell membrane crossing.[30] Cholesterol, a major sterol, assists the particle mainly in filling up bilayer defects, helper lipids to resemble the lipids in plasma membrane and PEG, a polymer, is mainly used to reduce further protein absorption to the particle. Moreover, it has been shown that multi-component LNPs are generally taken up by the cells efficiently.[8][10][31]

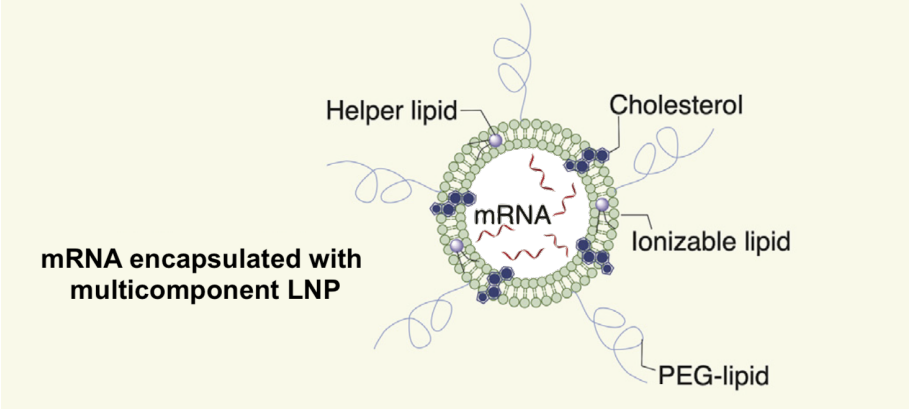

Figure 2.5: A multi-component lipid nanoparticle loaded with mRNA.[8]

There is much yet to be discovered when it comes to the mRNA delivery by LNPs, although it is generally accepted that the mRNA:LNP complexes are taken up by endocytosis. The mRNA:LNP is internalized by the recipient cell in early endosomes, which in the cytoplasm fuse with lysosomes, a vesicle containing digestive enzymes. In the acidic endosomal environment, the cationic lipids of LNPs fuse with the endosomal membrane releasing the RNA. Thereby, part of the mRNA molecules escape the endosomes and are released into the cytosol where they can be associated with ribosomes for translation. Some mRNA are also encapsulated by invagination of endosomal membrane to form, so called, intraluminal vesicles. These vesicles are secreted out of the cells and are referred to as extracellular vesicles of endosomal origin (endo-EVs). endo-EVs will then fuse with the adjacent cells and thus facilitate *in vivo* mRNA:LNP transport.[30]

3
Methodologies

Two different types of methodologies were developed in this thesis project, focusing on cell-specific protein expression after exogenous mRNA delivery: Mouse lung dissociation methods for *in vivo* applications and *in vitro* methods to study downstream protein expression after eGFP mRNA delivery to LA-4 cells and human lung tissue explants.

3.1 Lung dissociation

Methods to dissociate lung tissue often involve both mechanical and enzymatic tissue disruption to generate a single cell suspension. Mechanical dissociation is performed either by using a tissue grinder or manually by mincing the tissue with scissors and forceps. Extracellular matrix of a lung tissue is degraded enzymatically in order to get a single cell suspension. Dispase and collagenase are light proteases that have been proven efficient for digesting lung's extracellular matrix proteins but leaving important cell surface markers intact. Deoxyribonuclease (DNAse) is used to digest extracellular DNA released from dead cells in the dissociation process. Some examples of such enzymes with their catalyzing sites are presented in Table 3.1. Dispase II, collagenase III, collagenase/dispase and DNAse I are proteases on the market with different concentrations, specifically synthesized for certain tissue types. These proteases particularly digest the extracellular matrix and cell-released macromolecules such as DNA.

Table 3.1: Digestive enzymes and their corresponding reaction cites on tissue.

Digestive enzyme	**Catalyzing site**
Dispase	Fibronectin, type IV collagen, type V collagen [32]
Collagenase	Collagen fibers [33]
DNAse	Single- and double-stranded deoxyribonucleotides [34]

3.2 Flow cytometry

Flow cytometry is a method used to analyze the physical and chemical characteristics of a cell in fluid applying laser technology. The fluorescently labeled cell sample is focused to flow in a capillary that exposes one cell at a time through a laser beam that is scattered depending on the characteristics of the labeled cell. Forward

scattered light (FSC) corresponds to size of the cell, while the side scattered light (SSC) measures the morphological complexity. Dye-specific fluorescence signals are captured by the corresponding filters to measure the fraction of the fluorescence originating from labeling of cell-specific markers in the cell population. As visualized in Figure 3.1, the fluorescence signals are then converted into digital signals and processed by the computer connected physically to the instrument and by a software that handles the digital interface with the instrument.[35][36] Depending on the number of lasers and optimal filters contained in the flow cytometer, a number of cell characteristics can be analyzed simultaneously.

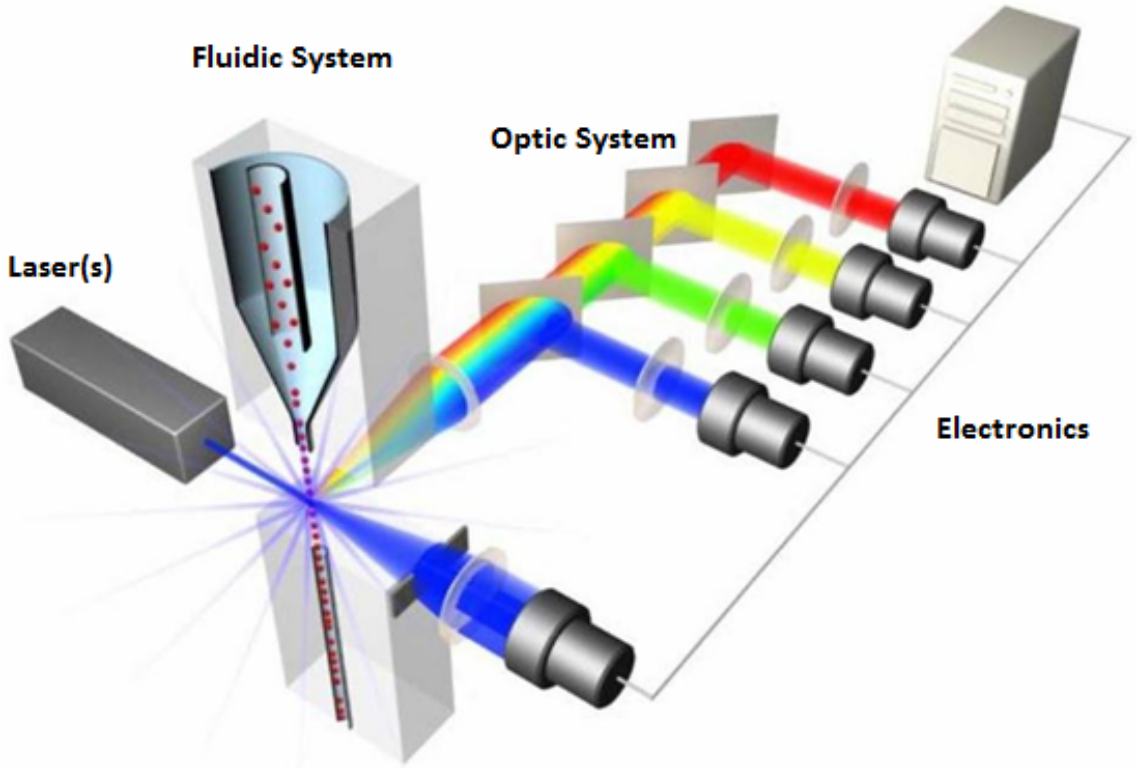

Figure 3.1: Basic principles of a flow cytometry. Excitation lasers meet the cells in the capillary, get scattered and the scattered light and fluorescent signals are captured by the use of different filters. The signals are converted into digital signals processed by a computer connected to the instrument.[37]

3.2.1 Compensation

Each fluorophore or staining dye has a broad spectrum of fluorescence that can overlap with the other fluorophores used in the same experiment. Compensation is a mathematical process to adjust for the spillovers caused by one fluorophore to another. The compensation is always calculated using single stain controls before analysis of the flow cytometry data.[36]

3.2.2 Fluorescence Minus One (FMO) control

To properly interpret flow cytometry analysis, FMO controls or isotype controls are often used. An isotype is an antibody with certain genetic variations and every antibody will have a specific isotype. A FMO or isotype control contains all the fluorophores in an experiment except the one that is tested, and this assists in the analysis to discriminate between background and positive staining.[35]

3.2.3 Data analysis

Flow cytometry data can be analyzed using a software for analyzing flow cytometry data such as FlowJo.[38] In this software, compensations can be set or corrected prior to analysis of the actual cell populations. The flow cytometry data for the corresponding samples can be plotted in two dimensions (for example a scattered plot of FSC vs SSC) or in one dimension to produce histograms of the different fluorophores. The regions containing populations of positives or negatives of the stains can be separated by creating a series of subsets or gates. Specific gating strategies exist for detecting different types of cell populations.[35]

3.2.4 Cell counting by flow cytometry

The cell number in a single cell suspension can be determined by adding a known concentration of counting beads. A diluted cell sample of unknown concentration with added beads is run in the flow cytometry to quantify the number of cells. The collected data can be analyzed in FlowJo to determine the concentration of the cells. The counting beads are brightly fluorescent in wide range of emission wavelength, so that the beads can be detected by several optical channels. In flow cytometry scatter plots, the population of beads fall in the minor scales of FSC and larger scales of SSC so that they are distinguishable from the cell populations. Calculation of the cell concentration is performed using Equation 3.1 after gating the populations of beads and cells respectively.[39]

$$\frac{A}{B} \cdot \frac{C}{D} = Concentration \tag{3.1}$$

Where:
A= number of cell events analyzed from FlowJo
B= number of beads events
C= assigned bead count of the lot (beads/ 25 µL)
D= volume if sample (µL)
The concentration of the sample is calculated as cells/µL

3.3 Cell real-time imaging

Cell real-time imaging techniques enables measurements of cell proliferation, cell morphology and fluorescence parameters over time in a non-invasive and non-pertubating

way to the cells. Its applications are wide, but in this thesis it was used to measure proliferation and eGFP protein expression after eGFP mRNA:Lipofectamine MessengerMAX transfection, enabling visualization of the time to protein translation on-set, total amount translated protein, the rate of translation and proportion of cultured mouse lung cells that are transfected. This in turn can assist in the understanding of the relationship between assay signal (eGFP protein expression and proliferation) and treatments (eGFP mRNA:Lipofectamine MessengerMax, in the future LNPs).[40]

3.3.1 Data analysis

Image data analysis of real-time imaging cell involves the design of masks over the objects by changing the radius, area and edge split of the objects to get an optimal mask that covers and detects the parameter intended, for example the cell area if it is a phase mask. Designed phase masks are interpreted by the software as cells and green masks as green fluorescence in order to process the images into data metrics. The analysis data can then be exported and visualized against time in graphs.[40]

3.4 eGFP mRNA transfection

LA-4 is a murine lung epithelial cell line, initially derived from neoplastic mouse lung epithelia. The cells have some properties of alveolar type II cells, except that they do not maintain a highly differentiated AT-II phenotype.[41]
Green fluorescent protein (GFP) is a protein that emits bright green fluorescence when exposed to light in the blue to ultraviolet range. GFP is widely used in biotechnology to measure the protein expression both qualitatively and quantitatively. The sensitivity of wildtype GFP expression in mammalian cells is quite low compared to standard reporter proteins. Enhanced green fluorescence protein (eGFP) is a modified GFP where amino acid changes have resulted in brighter signals.[42]
mRNA molecules can be delivered by using Lipofectamine MessengerMax as a carrier. Lipofectamine is a commercially available reagents, that is used in order to get an increased transfection efficiency and faster protein expression with no damage to the genome. Even though the cytotoxicity of the Lipofectamine MessengerMax, as tested with complexed RNA, was high, the cellular uptake of RNA was proven to be stronger in Lipofectamine MessengerMax-based delivery than polymer-based delivery.[16]

4

Materials and methods

Materials and methods describe the detailed experimental protocols developed in this thesis.

4.1 Mouse lung dissociation

Mouse lung dissociation experiments were performed with modifications in the protocols. Optimizations of the protocols were aimed to extract the highest number of epithelial cells. Flow cytometry with selected cell surface markers was used as a read-out in these experiments.
The total cell count of the samples and the mean frequency of live single cells with standard deviation between the duplicates were plotted using GraphPad Prism 8, a scientific graphing software.[43] The reagents used in lung dissociation experiments are presented in Table 4.1.

4.1.1 Initial lung dissociation experiments

Mouse lungs were obtained from female C57BL6/NCrl mice from the animal facility at AstraZeneca, the same strain that is currently used to conduct *in vivo* mRNA:LNP studies. All animal handling was performed by educated personal. The mice were anesthetized by intraperitoneal injection of pentobarbital (200 mg/mL, 0.2 mL mouse), and the lungs were removed without flushing the pulmonary circulation. The lungs were placed in cold phosphate buffered saline (PBS) and then transferred to the *in vitro* lab for further processing. Received lungs were dissected into lobes putting the left lobe and the inferior lobe into separate tubes in order to generate duplicates for every condition investigated. A diagram of mouse lung lobes is illustrated in Figure 4.1.
Enzymatic degradation was achieved by different enzyme combinations using dispase II, collagenase III, collagenase/dispase and DNAse I. A detailed protocol is found in Appendix A.1.1. Mechanical dissociation was achieved by using GentleMACS^{TM} Octo Dissociator, a tissue grinder with different programs, such as; *37C_m_LDK_1*, *m_impTumor_02* and *m_impTumor_03*. During the initial experiments, *37C_m_LDK_1* ran for 30 minutes with 37 °C heaters on.

After degrading the lung tissues mechanically and enzymatically, the samples were spun down at 310g for 5 minutes. The supernatants were discarded, the pellets were resuspended in 2 mL of ACK lysis buffer (Gibco^{TM}, A10492-01) and incubated

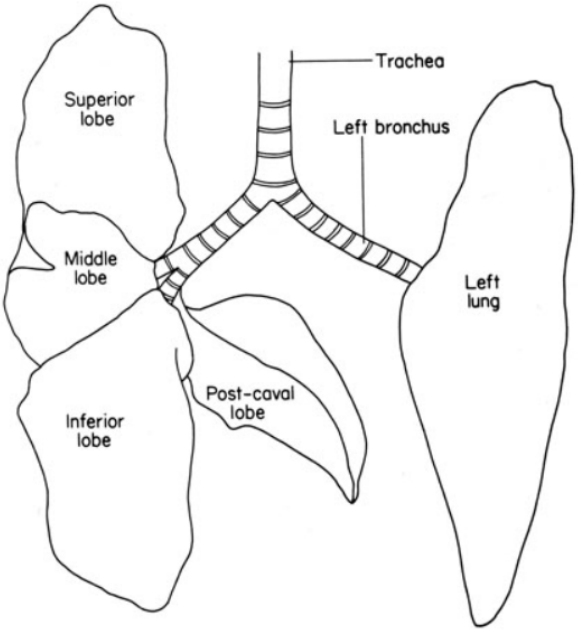

Figure 4.1: Gross anatomy of a laboratory mouse lung showing the lung lobes: four lobes to the right (superior, middle, inferior and post coval lobe) and one on the left (left lobe). The inferior lobe and left lung lobe were used for the initial lung dissociation, whereas all the lobes were used in the dispase method experiments.[44]

3-5 minutes to lyse the red blood cells. The lysis was stopped by adding 10 mL of FACS buffer (see Table 4.1 for the reagents in the buffer), the cells spun down at 350g for 8 minutes and the pellets resuspended in 2 mL of FACS buffer and filtered again through a 100 µm cell strainer to proceed with staining and subsequent flow cytometry analysis.

4.1.2 Dispase method

In the dispase method, the mice were anesthetized by intraperitoneal injection of pentobarbital (200 mg/mL, 0.2 mL mouse). The pulmonary circulation was then flushed with cold PBS by an incision made in the left atrium for drainage (right ventricle, 27G needle, 10 mL ice cold PBS). This procedure made the flushed lungs blanched with some variation. The lungs were then inflated with around 2 ml of dispase solution (50U/mL, room-temperatured, Corning 354235) via the tracheal cannula and the trachea tied off to retain the enzyme solution prior to lung removal. The lungs were placed in cold PBS and then transferred to the *in vitro* lab for further processing. The lungs were then dissected into lobes and placed in GentleMACS C tubes containing DNAse I and collagenase/dispase solution, where the left lung lobe was separated from all of the right lobes and the lobes were placed into two separate tubes.

In the initial dispase experiment only one digestion Protocol was used combined with mechanichal dissociation using the GentleMACS^{TM} Octo Dissociator. The programs used in these experiments were *m_impTumor_02* and *m_impTumor_03*, both involving around 30 s mechanical dissociation, with 40 minutes incubation period of the samples at 37°C in between. Collagenase/dispase dissolved in PBS was added to the samples before *m_impTumor_02* and DNAse I which was added 10

minutes prior to the dissociator program *m_impTumor_03*.

In the final experiment, all of the samples containing initial enzyme combinations (3 Protocols) were treated with the dispase method. Manual mincing was performed parallel to the dissociator digestion with sterile scissors, forceps and syringe plunger to mash the enzymatically digested tissue before filtering through the cell strainer. Enzymatic degradation was performed by 3 different combinations of enzymes, which is presented in detail in Appendix A.1.2.

4.1.3 Cell counting

CountBright^{TM} Absolute counting beads (Invitrogen, C36950) were used to measure the cell concentration in the generated mouse lung cell suspensions. 100 µL of the cell samples were added with 25 µL of the counting beads and 50 µL of CD45 antibody (see Table 4.2) for further verification and the samples were run on flow cytometry. The total amount of cells in each sample was calculated according to Equation 3.1, described in methodologies.
To confirm cell counts generated using CountBright Absolute counting beads in the final experiment, the generated cell suspensions were also counted using Sysmex XP-300™[45], a cell counter primarily used for hematology samples.

4.1.4 Staining and data acquisition

4-color panel
$3 \cdot 10^6$ cells/ lung sample were added in FACS tubes and washed with 1 mL of PBS to remove fetal bovine serum (FBS), included in the FACS buffer. The samples were spun at 350g for 10 minutes and the pellets were resuspended with 1:1000 of eBioscience^{TM} Fixable viability dye eFluor^{TM} 780 (live/dead) (Invitrogen, 65-0865-14) to stain the dead cells and 1:100 FC block (Purified rat anti-mouse CD16/CD32) to inhibit non-specific bindings during subsequent antibody staining.[35] The samples were incubated for 15 minutes in a dark room at room temperature (RT), washed with 200 µL of FACS buffer and spun down at 350g for 5 minutes. After discarding the supernatent, the pelleted cells were resuspended in 50 µL antibody mix containing the antibodies and dilutions described in Table 4.2. Staining was performed at 4°C for 30 minutes. The samples were then washed twice with 200 µL of FACS buffer, spun down at 350g for 5 minutes and pellets resuspended with 200 µL of FACS buffer prior to flow cytometry analysis. Compensation controls were generated using UltraComp eBeads^{TM} (eBioscience, 01-2222-41) for antibodies but cells for live/dead dye.
Data acquisition was performed on a BD Accuri^{TM} C6 Plus instrument (Becton, Dickinson & Company), a flow cytometer with a blue (488 nm) and red (640 nm) laser, able to analyse a maximum of four different fluorophores. Data analysis, including compensation, was performed using FlowJo analyzing software version 10.6.1 (Becton, Dickinson & Company).
Isotype controls were included in the FMO controls for the final experiment to strengthen the cell identifications. An example of a set of FMO controls used on

the last experiments is presented in Appendix A.1.3.

8-color panel
In the extended staining panel, applied to the samples from the final lung dissociation experiment of dispase method, live/dead and surface antibody staining was performed as described above for the 4-color panel but using the antibodies listed in Table 4.3. After surface staining, the cells were again pelleted by centrifugation, 350g for 5 min, and the cells were then fixed and permeabilised for intracellular staining (both cytoplasm and nuclear) by addition of 100 µL of Transcription Factor Staining Buffer set (eBioscience, 00-5523) according to manufacturer's instructions. Briefly, the cells were incubated over night in Fix/Permiabilisation Buffer, washed twice the next day with the permeabilisation buffer. After a second wash, the cells were resuspended, blocked with FC-block for 15 min (25 µL of 1:100 FC-block, 15 min, RT) before addition of intracellular staining mix (100 µL of pro-SPC 1:50 diluted in permeabilisation buffer) followed by another 45 min of incubation in RT, in dark. The cells were then washed with two subsequent washes with permeabilisation buffer before addition of 50 µL of BV421 goat anti-rabbit IgG (H+L) (BD 565014) (secondary antibody), diluted 1:200 in permeabilisation buffer for 30 min, RT in dark. The cells were then washed twice and resuspended in 300 µL of FACS buffer for acquisition on a BD LSRFortessa^{TM} 4L instrument (company), a flow cytometer with violet (405 nm), blue (488 nm), green (561 nm) and red (640 nm) lasers that can detect up to 16 colors simultaneously. All samples were filtered immediately before acquisition to prevent clogging in the flow cytometer. Compensation controls were generated by incubating 20 µL of UltraComp eBeads (eBioscience) with 1 µL of the different antibodies. Only unstained and Fixable Live/Dead compensation controls were generated using a pool of cells.

Table 4.1: Reagent list for the lung dissociation experiments.

Name	**Vendor**	**Concentration (stock)**	**Catalog number**
CountBright Absolute absolute counting beads	Invitrogen	0.5E5/50uL	C36950
UltraComp eBeads ^{TM}	Invitrogen	25test (50uL/test)	01-2222-41
eBioscience ^{TM} Fixable viability dye eFluor ^{TM} 780	Invitrogen	1000x	65-0865
Gibco^{TM} ACK lysing buffer	Gibco^{TM}	1x	A10492-01
Corning ® cell strainer	Sigmaaldrich	100um	CLS431751-50EA
PBS	Gibco ^{TM}	100mL	70011-036
Fix/Perm Buffer	eBioscience		00-5523
FACS buffer		**Dublecco's PBS; 2% FBS-HI; 2mM EDTA**	
Dublecco's PBS	Gibco^{TM}	1x	14190-094
FBS Heat inactivated	Gibco^{TM}		10438-026
Ultrapure EDTA	Invitrogen	0.5M	15575-038
Enzymes			
Deoxyribonuclease I	Invitrogen	187 U/ uL, stock	18047019
Dispase	Corning	50U/mL, unknown	354235
Dispase ® II (neutral protease, grade II)	sigmaaldrich	0,9U/mg, stock 10mg/mL	4942078001
Collagenase/Dispase	Roche	100mg, stock 100 mg/ml	10269638001
Collagenase Type III	worthington	172U/mg, stock 10mg/mL	BX33223

Table 4.2: 4-color staining panel antibodies with coupled fluorophores to corresponding optical filters and the lasers of BD Accuri^{TM} C6 Plus flow cytometry to detect key cell types [21].

Antibody	**Clone**	**Cell type**	**fluorophore**	**Vendor**	**Dilution**	**Optical filter**	**Laser**
CD45	30-F11	Hematopoietic cells	FITC	BD	1:400	533/30	488nm
CD31	MEC 13.3	Endothelial cells	PE	BD	1:100	585/40	488nm
CD326	G8.8	Epithelial cells	APC	BD	1:100	675/25	640nm
Fixable viability dye		Dead cells	eFluor 780	Invitrogen	1:1000	670 LP	640nm

Table 4.3: 8-color staining panel antibodies with coupled dyes and detected cell types with corresponding optical filters and laser used in BD LSRFortessa^{TM} flow cytometry.

Antibody	**Clone**	**Cell type**	**fluorophore**	**Vendor**	**Dilution**	**Optical filter**	**Laser**
ProSPC	MEC 13.3	Alveolar type II cells	Unconjugated	BD	1:100		
Goat anti-rabbit IgG (H+L)			BV421	BD	1:200	450/50	405nm
CD45	30-F11	Hematopoietic cells	BV650	BD	1:400	670/30	405nm
CD74	In-1	Alveolar type II cells	BV786	BD	1:100	780/60	405nm
F4/80	Cl:A3-1	Macrophages	FITC	Serotec	1:200	530/30	488nm
CD31	MEC 13.3	Endothelial cells	PerCP-Cy5.5	BD	1:400	710/50	488nm
CD326	cG8.8	Epithelial cells	PE	BD	1:100	586/15	561nm
podoplanin (T1a)	8.1.1	Alveolar type I cells	APC	Biolegend	1:200	670/14	640nm
Fixable viability dye		Dead cells	eFluor 780	Invitrogen	1:1000	780/60	640nm

4.2 Real-time cell analysis to monitor eGFP mRNA translation in LA-4 cells

In order to study the dynamics of protein translation after mRNA delivery *in vitro*, LA-4 cells were cultivated and transfected with eGFP mRNA.

4.2.1 LA4-cell culture

LA-4, a mouse lung epithelial cell line, was purchased from ATCC (CCL-196).[46] The cells were expanded in a $175cm^2$ flask containing 35 mL of Ham's F-12 Nut Mix + GLUTAMAX medium supplemented with FBS, non-essensiatial amino acids (NEAA) and penicillin/streptavidin antibiotics, see Table 4.4 for detailed description. 24h prior to eGFP mRNA transfection, the cells were rinsed with PBS to remove traces of FBS that contains trypsin inhibitor and deattached using Accutase, a digestive enzyme. The cells were then seeded into 96-well plate at different cell densities, 18-24 hours prior to the transfection with eGFP:Lipofectamine, see Figure 4.2 for the layout of the 96-well plate. A detailed reagent list for the cell culture is presented in Table 4.5.

Table 4.4: Growth medium of LA4 cells with supplements and their concentrations.

Reagent	**Concentration (stock)**	**Volume** (mL)	**Final concentration** (***V/V %***)
Ham's F-12 Nut Mix + GLUTAMAX	1x	415	100%
FBS	1x	75	15%
MEM NEAA	100x	5	1%
PenStrep	100x	5	1%

Table 4.5: Reagent list for eGFP mRNA transfection in LA-4 cells.

Name	**Vendor**	**Catalog number**
Nunc EasYFlask 75 cm^2	ThermoFisher Scientific	156499
StemPro Accutase	Gibco^{TM}	A11105-01
96-well plate Croning Falcon Blk/Clr	BD	354640
F-12 Nut Mix + GlutaMAX	Gibco^{TM}	31765
PenStrep 10 kU/ml	Gibco^{TM}	15140-122
FBS	Gibco^{TM}	10270-106
MEM NEAA 100X	Gibco^{TM}	11140-050
DPBS	Gibco^{TM}	14190-094
Lipofectamine ® MessengerMax	Invitrogen	18324010
eGFP mRNA	TriLink	L-7201-100
Fix/Perm Buffer	eBioscience	00-5523
Dublecco's PBS	Gibco^{TM}	14190-094
FBS Heat inactivated	Gibco^{TM}	10438-026
Ultrapure EDTA	Invitrogen	15575-038

4.2.2 eGFP mRNA:Lipofectamine MessengerMax transfection in LA-4 cells

For efficient mRNA delivery to the cells, mRNA sequence encoding eGFP from TriLink Biotechnologies was complexed with with Lipofectamine MessengerMax (Thermoscientific, LMRNA003). Ratio of Lipofectamine:mRNA in the transfection reagent was 3:2. The mRNA:Lipofectamine MessengerMax lipoplexes were generated at highest mRNA concentration and then serially diluted down to 3.9 ng/cm^2. To prepare the initial concentration, mRNA, dissolved in dH_2O and Lipofectamine MessengerMax, diluted in serum-free F-12 Nut Mix medium were incubated at RT for 10 minutes. Then the mRNA solution was added to the Lipofectamine MessengerMax solution and the reagent was incubated again at RT for 5 minutes prior to the transfection.
In the second experiment, mRNA:Lipofectamine MessengerMax reagents were mixed into the medium prior to addition to the cells. In the first experiment the transfection reagents were added in a 25 µL volume to the edges of the wells with LA-4 cells.

	1	2	3	4	5	6	7	8	9	10	11	12
A	PBS	PBS	PBS	PBS	PBS	PBS	PBS	PBS	PBS	PBS	PBS	PBS
B	PBS	1000	500	250	125	62.5	31.25	15.6	7.8	3.9	UT	PBS
C	PBS	1000	500	250	125	62.5	31.25	15.6	7.8	3.9	UT	PBS
D	PBS	1000	500	250	125	62.5	31.25	15.6	7.8	3.9	UT	PBS
E	PBS	1000	500	250	125	62.5	31.25	15.6	7.8	3.9	UT	PBS
F	PBS	1000	500	250	125	62.5	31.25	15.6	7.8	3.9	UT	PBS
G	PBS	1000	500	250	125	62.5	31.25	15.6	7.8	3.9	UT	PBS
H	PBS	PBS	PBS	PBS	PBS	PBS	PBS	PBS	PBS	PBS	PBS	PBS

Figure 4.2: Layout of the 96-well plate for the eGFP mRNA transfection experiment of LA-4 cells, where cell densities were 5000, 10 000 and 20 000 cells/well (two rows per density) and mRNA concentration varies 1000 - 3.9 ng/cm^2 column-wise. UT denotes the negative control where no lipoplexes were added. Doses refer to *ng* mRNA per surface area of the well bottom where the cells were cultivated (96-well plate).

4.2.3 Data acquisition and analysis

The readout of this set of experiments was fluorescence signal derived from a live-cell analysis system called IncuCyte S3 that analyzes the eGFP expression together with the cell growth rate both qualitatively and quantitatively.[40] Transfected 96-well plates were loaded in IncuCyte S3 to measure eGFP protein expression and cell growth over time. The Incucyte S3 2019A software was used to analyze the data generated. The software was set to generate four images per well at 10X magnification every 2 hours. IncuCyte S3 had a GFP channel to collect eGFP expression signals and a phase channel to analyze the cell morphology and growth rate. For data analysis, masks over both the channels were designed as illustrated

in Figure 4.3. Identical masks were used in all experiments performed.

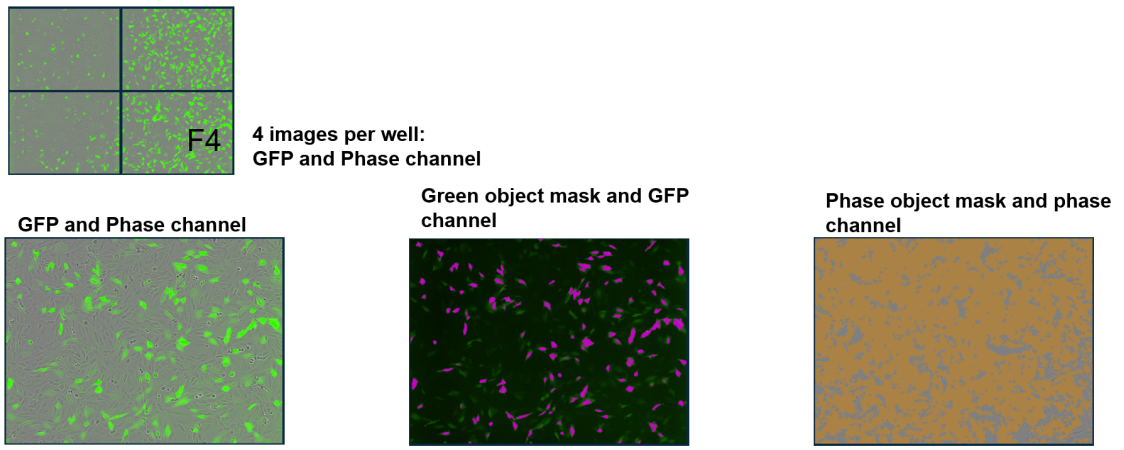

Figure 4.3: Overview of IncuCyte S3 analysis. top left: one well (F4 = 20 000 cells/well with 250 ng/cm^2 dosage from Experiment 1) is divided in to four images and GFP and phase channels are shown. bottom left: one of the four images with GFP and phase channel turned on. bottom middle: the same image with designed green masks and GFP channel are shown. bottom right: The image with phase channel turned on, showing the designed phase masks.

Once the masks are designed, different metrics were calculated and the data were exported to using GraphPad Prism 8 for visualization in plots. "Total integrated intensity" is a metric that shows the total sum of the objects' fluorescence intensity in the image, which can be simplified as the total signal of eGFP protein expression per cell. "Green area/ phase area" in percentage is another metric that shows the area of GFP mask normalized with the area of phase mask, which can be interpreted as the fraction of eGFP expressing cells in this experiment. "Confluency" is also a metric that shows the object count over an image with time which is simply the growth rate of the cell culture.

In experiment-2, median fluorescence intensity (MFI) of transfected LA-4 cells and percentage of eGFP expressing cells were also measured using flow cytometry, 24 hours after the transfection as the expression plateaued by that timepoint. The cells were washed with 150 µL of PBS and detached from the surface by adding 100 µL of Accutase and incubating the plate 5-10 minutes in 37 °C. After inspecting the detached cells in the microscope, the Accutase reaction was stopped by adding 150 µL of cell growth medium per well. The duplicate samples were pooled into a single sample for the different mRNA doses to increase the number of cells per sample. The samples were centrifuged at 350g for 5 minutes in RT. The pellets were then thoroughly resuspended in 200 µL of freshly made Fix/Perm buffer (eBioscience, 00-5523) and incubated in RT for 30-60 minutes. The samples were washed two times with 1 mL of FACS buffer and spun down at 600g for 8 minutes. At the end, the cell pellets were resuspended in 200 µL of FACS buffer and analyzed flow cytomtry. eGFP was detected by corresponding filter of FITC on BD Accuri^{TM} C6 Plus flow

cytometry. The acquired data was analyzed using FlowJo and results were plotted in GraphPad Prism 8.

4.3 eGFP mRNA transfection in human lung tissue

eGFP:Lipofectamine MessengerMAX transfection of human lung tissues was also tested with the aim to construct a human *in vitro* model that can predict mRNA:LNP uptake by different human lung cells. Reagents used in this experiment are presented in Table 4.6. Fresh non-cancerous human lung tissue received from lung cancer patients was minced into small cubes of up to 3 mm^2 in size with sterile scissors and forceps in a petridish containing PBS. The pieces were added to a 96-well plate (costar, 3799), 1-3 pieces/well in 250 ul X-Vivo 10 medium, following the layout in Figure 4.4. The tissue pieces were then left to rest overnight at 37 °C prior to eGFP transfection. The next day, the lung pieces were transferred to a new plate with 100 µL X-vivo medium and transfected with mRNA:Lipofectamine MessengerMAX reagents at mRNA eGFP doses of 250 - 4000 ng/cm^2, as seen in Figure 4.4. The reagents had been prepared in serum-free PBS similarly to what is descirbe in the LA-4 section, and the highest dose was now 4000 ng/cm2. 24 hours after the transfection, the samples were homogenized in 400 µL of 1X cell extraction buffer (Abcam, from the ELISA kit ab171581), including protease inhibitors (Complete EDTA free protease inhibitor cocktail, Sigma Aldrich 11873580001) in a FastPrep-24 (MP Biomedicals) at 4 m/s, 3 times 15 seconds with 5 minutes of cooling on ice between rounds. The homogenates were centrifuged at 18000g at 4 °C for 20 minutes. The supernatants were collected and analyzed with eGFP ELISA kit for quantitative measurements of eGFP protein and with Pierce^{TM} BCA total protein assay kit (Thermofisher, 23227) for total protein concentrations. The results were then plotted using GraphPad Prism 8.

	1	2	3	4	5	6	7	8	9	10	11	12
A		ng/cm2										
B		4000	2000	1000	500	250	UT	1 piece				
C		4000	2000	1000	500	250	UT	2 pieces				
D		4000	2000	1000	500	250	UT	3 pieces				
E												
F												
G												
H												

Figure 4.4: Layout of the 96-well plate for the eGFP mRNA transfection experiment on human lung tissue explant, where rows B-D had 1-3 tissue pieces respectively and the transfection reagent was added in a concentration that differed from 4000-250 ng/cm^2.

.

Table 4.6: Reagents used in eGFP mRNA transfection in human lung explant experiments.

Material	**Vendor**	**Catalog number**
X-Vivo 10 medium	Lonza	BE04-743Q
PBS without Ca^{2+}, Mg^{2+}	Gibco^{TM}	10010-015
Penicillin-Streptomycin	Gibco^{TM}	15140-122
L-glutamine	Gibco^{TM}	25030081
Lipofectamine MessegerMAX	Invitrogen	18324010
eGFP mRNA	Trilink	L-7201-100
Complete EDTA free protease inhibitor cocktail	Roche	11873580001
GFP ELISA kit	Abcam	ab171581
Ceramic beads, Lysing Matrix D	MP Biomedicals	6913-500
Pierce BCA Protein Assay kit	ThermoScientific	23227

5
Results and discussion

5.1 Mouse lung dissociation

Lung tissue processing is complicated because of the numerous cellular compartments. Here, the generation of a single cell suspension for flow cytometry analysis with optimal cell numbers and viability was sought to be optimized. The particular interest of designing the protocols was to extract lung epithelial cells. Generation of a single cell suspension of epithelial cells is complicated due to their adherence to the basement membrane. Protocols for the lung dissociation were designed based on literature and previous experience at AstraZeneca. The mouse lung single cell suspensions generated were stained with markers against hematopoietic cells, endothelial cells and epithelial cells as listed in Table 4.2.

5.1.1 Initial lung dissociation

As a starting point for mouse lung dissociation, three Protocols that had been validated and/or developed in-house at AstraZeneca were used. One of the Protocols was composed of a kit (Miltenyi Biotec cite [47]), containing an unknown enzyme mixture, used in-house as a standard method to extract lung immune cells. This method was compared against two other in-house Protocols that had previously been used to extract non-immune lung cells containing different mixtures of collagenase and dispase.
For mechanical dissociation, we initially used only the GentleMACS^{TM} Octo Dissociator, program *37C_m_LDK_1*. The flow chart below provides an overview of the designed Protocols for initial mouse lung dissociation. A detailed protocol with the concentrations of different enzymes are presented in Appendix A.1.1.

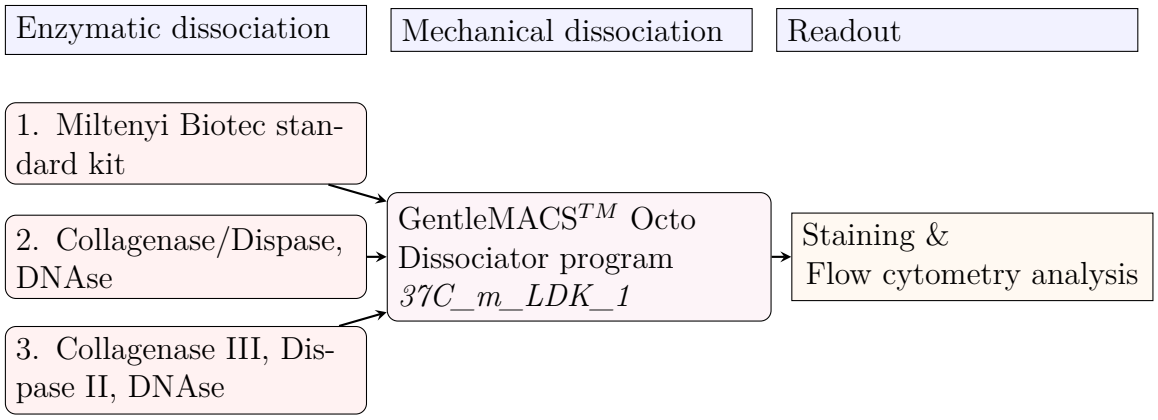

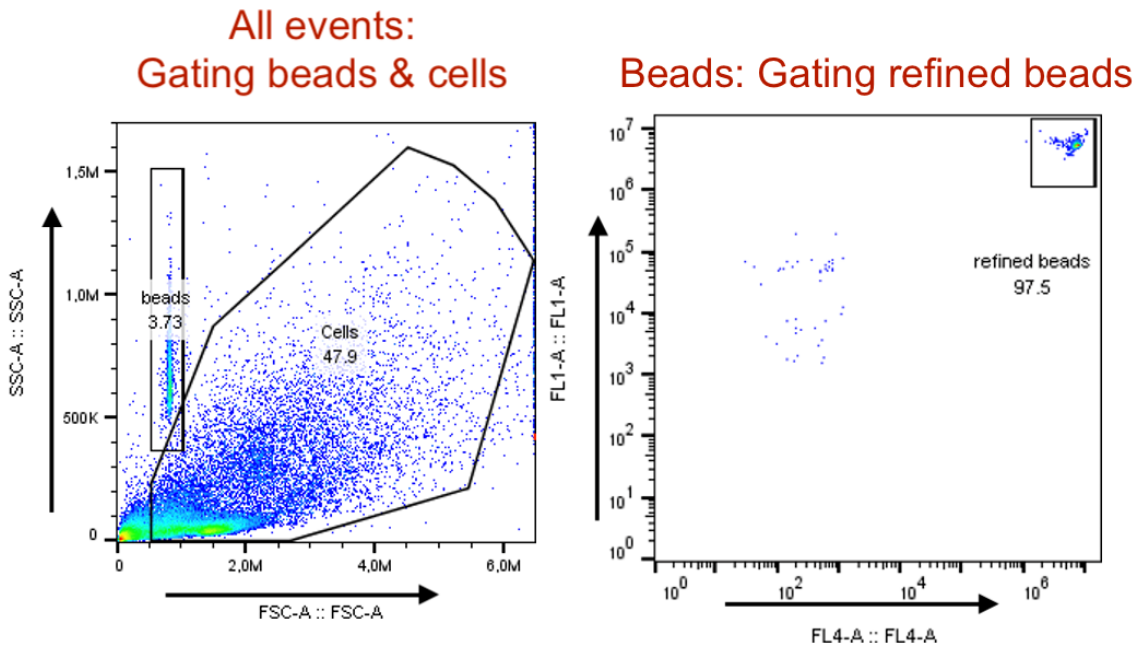

Figure 5.1: Gating strategy to gate the counting beads & cells: All events → beads & cells; Beads→ Refined beads.

Throughout the lung dissociation, cell counting was performed using CountBright Absolute Counting Beads in flow cytometry. Acquired data was analyzed using FlowJo and a gating strategy used is presented in Figure 5.1. The cell counts of the initial lung dissociation experiments are illustrated in Figure 5.2.
The total cell yield (sum of left and right lobes) of the mouse lungs for protocol 2 and 3 were as low as $2.3 - 2.8 \cdot 10^6$, compared to the results in the order of 10^7 that *Benjamin et al 2016* [48] present. It was believed that the initial recovery of cells had been higher, however at what stage a high proportion of cells had been lost could not be fully determined. The total cell count from protocol 1 was reasonable.
A 4-color panel staining with markers against hematopoietic cells, endothelial cells and epithelial cells was used throughout the experiments. The FlowJo software was used to analyze the data and to calculate the compensation matrix. The gating strategy applied is visualized in Figure 5.3, adapted from *Benjamin et al 2016.*[48] Compensation matrix was calculated and applied to all the samples in FlowJo.
Flow cytometry analyzed cell fractions are presented in Figure 5.4. A proportion of CD45+ cells (hematopoietic cells) were also positive for CD326+ or CD31+. It is not known what these cells are, but one possibility is unspecific staining of macrophages.
Despite the lack of replicates in these initial lung dissociation experiments, the conclusion was that the frequency and number of epithelial cells were really low (state frequency) and it is needed to seek other methods to increase the recovery of lung epithelial cells. Then a literature study was conducted to search for alternative methods that would enable a dissociation to yield a single cell suspension with high epithelial cell fraction.

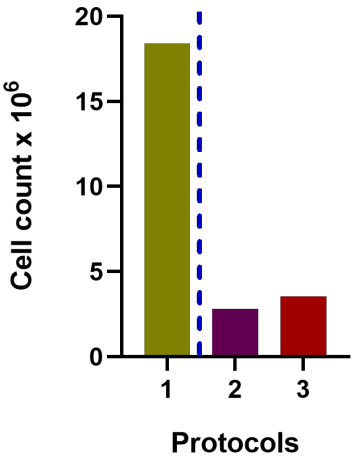

Figure 5.2: Cell count from the initial two lung dissociation experiments, using CountBright Absolute counting beads. Presented is the sum of the cell counts obtained from the left and right lung lobes. The data for protocol 1 was generated in a consecutive experiment and these cells were counted using a new batch of counting beads.

5.1.2 Dispase method

Next a combination of initial lung dissociation Protocol 2 with an *in vivo* dispase method was tested. In this protocol, two steps *in vivo* were added. First, the pulmonary circulation was flushed with PBS to remove blood. Secondly, the lungs were inflated with 2 ml of dispase solution and the trachea tied prior to lung removal at the animal house and then further processed *ex vivo* with Protocol 2 enzyme mixture similar to that of the initial lung dissociation. However, concentration of collagenase/dispase was increased this time, but the concentration of DNAse I was kept the same as before. As is visualized in the flowchart below, two different GentleMACS^{TM} Octo Dissociator programs (*m_impTumor_02* and *m_impTumor_03*) were used without heater. As read-out, the 4-color panel was used to visualize the cell population.

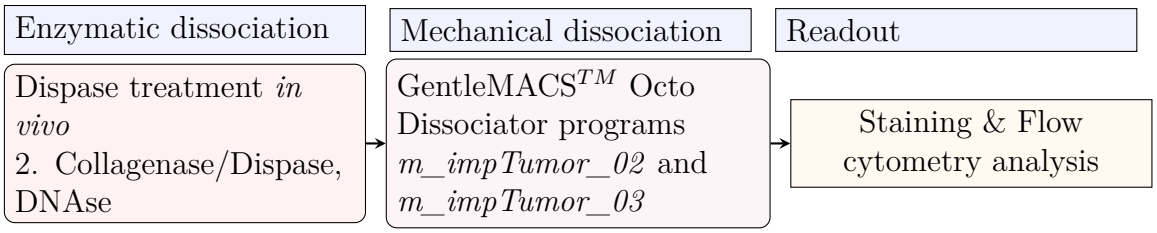

The lungs appeared paler than in previous experiments, as the excess of RBC had been flushed out. The cell count and the frequencies of key cell types generated using Protocol 2 are given in Figure 5.5.

Initial experiment of dispase method results show that the additional dispase treatment *in vivo* increased the frequency and thus, the number of epithelial cells extracted was also elevated, namely 8% of the single cell solution. Even the cell total count was reasonable. Therefore, it was concluded to repeat the *in vivo* dispase treatment applying the three enzymatic conditions previously used.

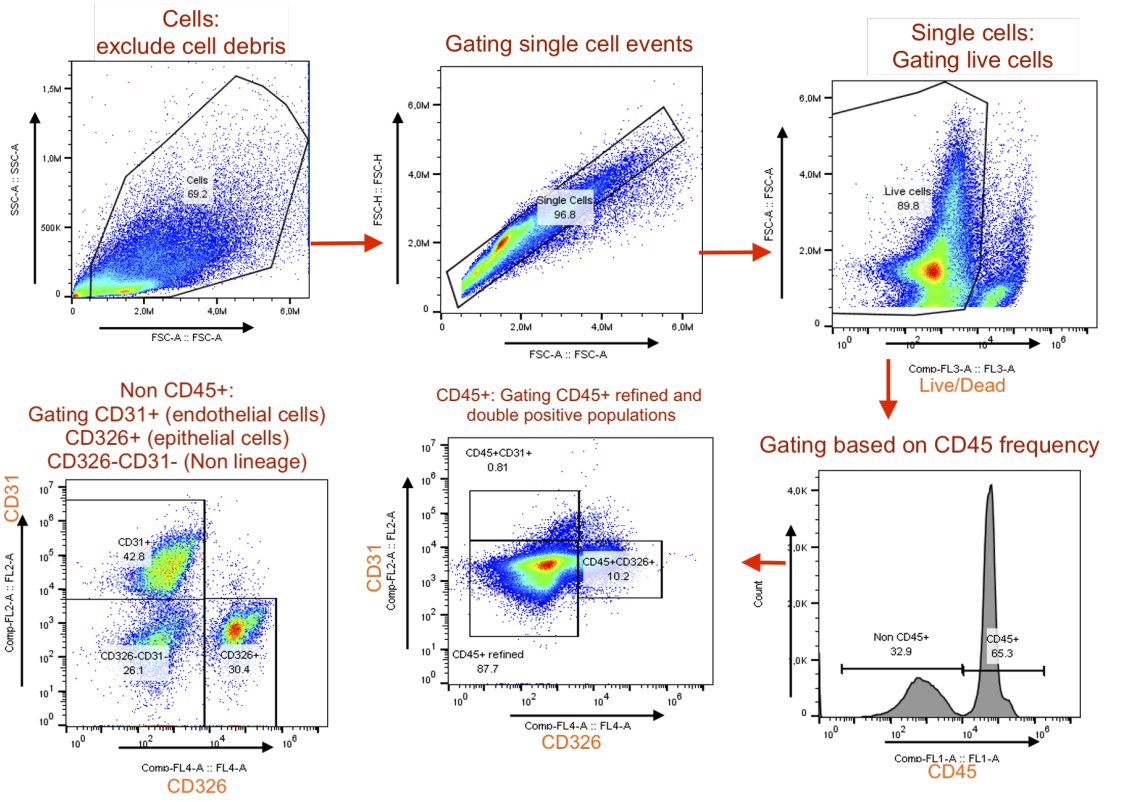

Figure 5.3: Gating strategy applied to the 4-colour panel. The cells were first visualized in scatter plots based on FSC-Area (FSC-A) against SSC-Area (SSC-A) to gate the cell populations excluding debris of low FSC-A axis. Single cells were then selected using FSC-A against FSC-Height (FSC-H). Gating of live cells was done in a scatter plot visualising FSC-A against live/dead axis (positive staining indicating dead cells). The live cells visualized in a histogram of CD45 axis gated for CD45 positive and negative cells. Visualizing the CD45 positive population in scatter plot, double positive populations and refined CD45+ populations were gated. CD45 negative cells were used to further gate CD31 positive, CD326 positive and non-lineage positive cell populations.

As presented in the flowchart below, two different GentleMACS^{TM} Octo Dissociator programs were run. Together with the GentleMACS^{TM} Octo Dissociator programs m_impTumor_02 and m_impTumor_03, manual mincing was also performed for another half of the samples in parallel. The manual mincing was performed using sterile scissors and forceps in the beginning and mashing with syringe plunger during filtering the samples and an overview of this protocol is presented in the flowchart below. A detailed protocol can be found in Appendix A.1.2. In addition, an 8-color flow cytometer panel was included to further characterize the epithelial cells extracted.

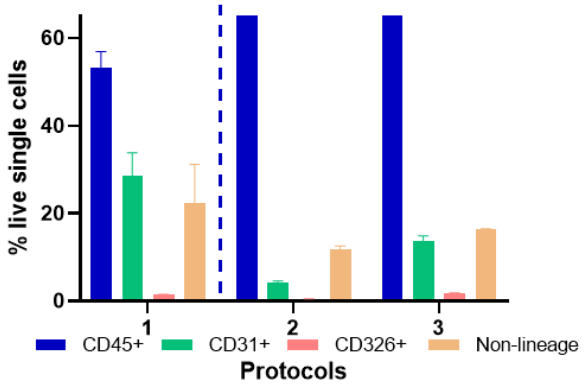

Figure 5.4: Frequency of live cell populations (mean of the duplicates) of live single cells from the initial lung dissociation, where protocol.1 experiment was performed on a separate occasion: hematopoietic cells (CD45+), endothelial cells (CD31+), epithelial cells (CD326+) and non-lineage cells (CD326-CD31-CD45-).

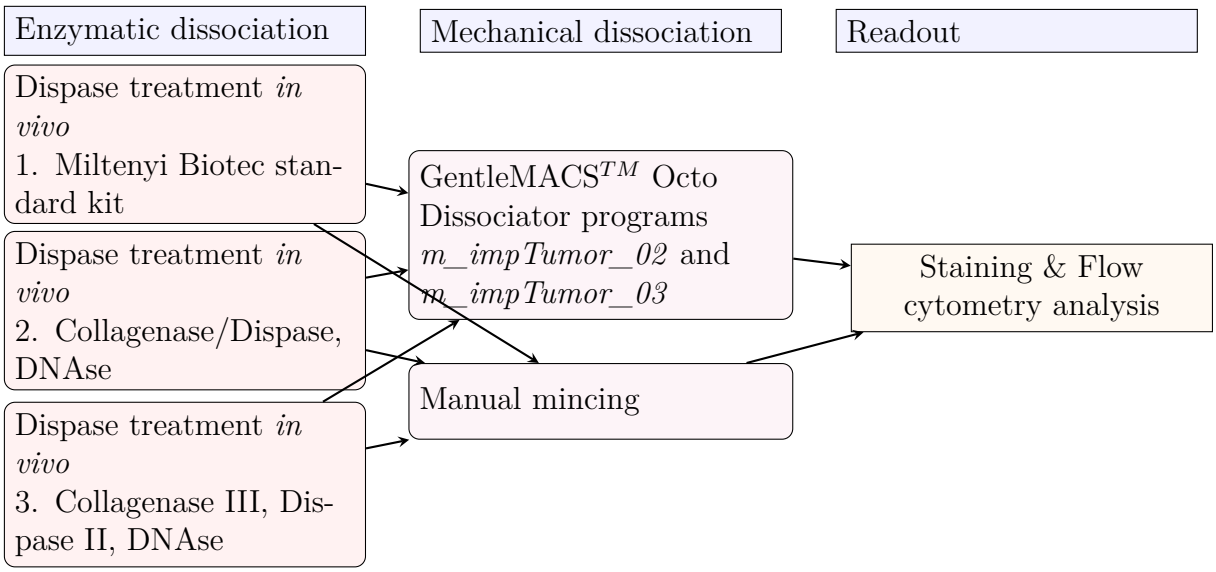

During the extended panel of lung dissociation, following the protocol design presented in the flow chart, the cells were also counted manually using Sysmex hematometer to confirm the cell counts from counting beads, which is found in Appendix A.1.5. The hematometer count results were somewhat similar to that of measured with the counting beads, which is presented in Figure 5.6.
The overall cell recovery was high in all protocols, however highest cell counts were achieved with Protocol 3:Manual mincing (Collagenase III, Dispase II). This Protocol also had the highest frequency of epithelial cells (13-14%). The epithelial cell frequency in one of the samples from 2:Manual mincing Protocol is contradicting from the other results for unknown reason, which is explicitly visible in the plot.

Viability of different cell types was also investigated in the 4 color staining panels and the results are presented in Table 5.1. Hematopoietic cells did not show big variations between the Protocols. Protocol 2 with dissociator gives better viability for all of the cell types in the dispase method. Endothelial cells show significant variations in viability depending on the Protocols and have better viability in the *in vivo* dispase method Protocol 2 with both manual mincing and GentleMACS^{TM} Octo dissociator program. Protocols with manual mincing seems to favor the via-

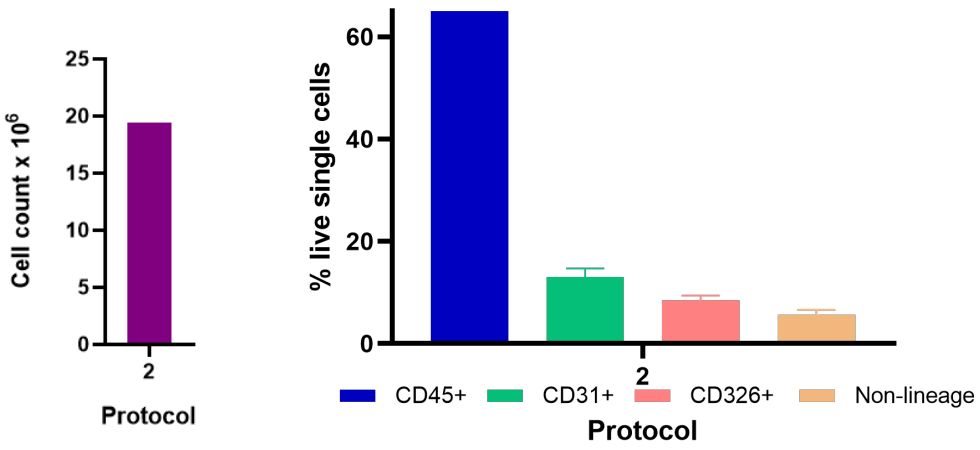

Figure 5.5: Results from Protocol 3 of the dispase method lung dissociation. Left: Total cell count using CountBright Absolute counting beads on flow cytometry. Right: Frequency of live hematopoietic cells (CD45+), endothelial cells (FITC-CD45+), epithelial cells (CD326+) and non-lineage cells (CD326-CD31-CD45-) in the single cell suspension.

bility of epithelial cells, compared to the dissociator treatment in dispase method. Still, more experiments on the Protocols are necessary to optimize the cell viability.

In the final dissociation experiment performed, the 8-color staining panel was included to investigate the recovery of alveolar type I and II cells in the epithelial population. ProSPC and CD74 were markers tested for labelling AT-II cells and Podoplanin or T1a was used to label AT-I cells. An F4/80 antibody, a marker for the macrophages, was also used in the panel, since this population is often seen as highly auto-fluorescent.

The gating strategy for 8-color panel is presented in Figure 5.7. CD326+ cell population was gated exactly as for the 4-color panels. ProSPC positive population was gated from the CD326+ cells and the results can be found in Appendix A.1.4. Unfortunately, CD74 could only be found in the dead cell population, but these cells also stained positive for ProSPC. No population for AT-I podoplanin positive population could be identified. The Protocols did not extract as much as AT-I cells, which are less in number in the lungs.

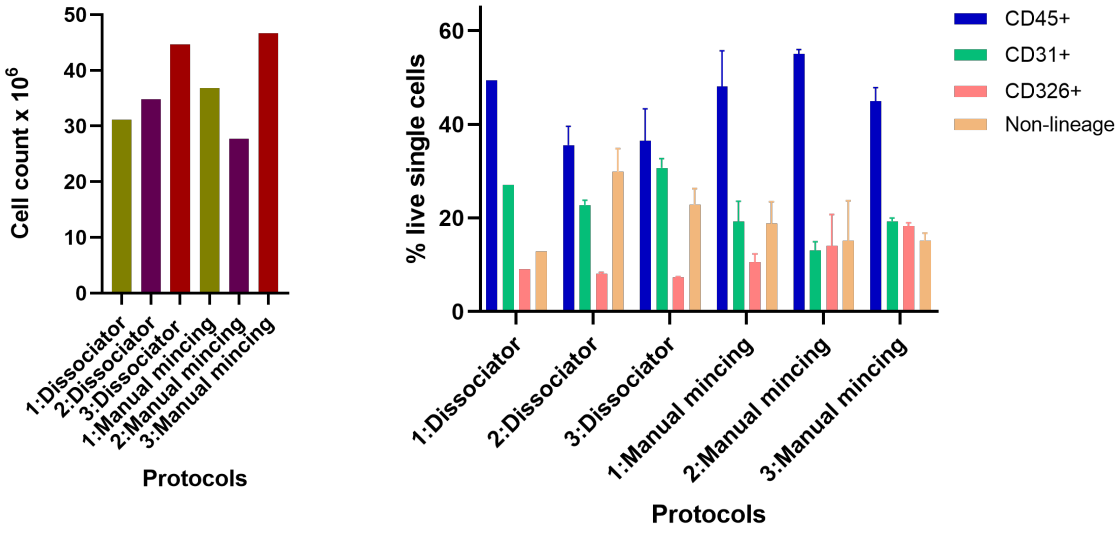

Figure 5.6: Cell counts and cellular fractions from the final mouse lung dissociation experiment applying the *in vivo* dispase method. Left: Total cell count using flow cytometry with CountBright Absolute counting beads. Right: Frequency of live hematopoietic cells (CD45+), endothelial cells (CD31+), epithelial cells (CD326+) and non-lineage cells (CD326-CD31-CD45-) in the single cell suspension.
(Note! Staining on one of the samples from 1:dissociator Protocol went wrong, therefore this Protocol is only represented by one replicate, thus no STDs.)

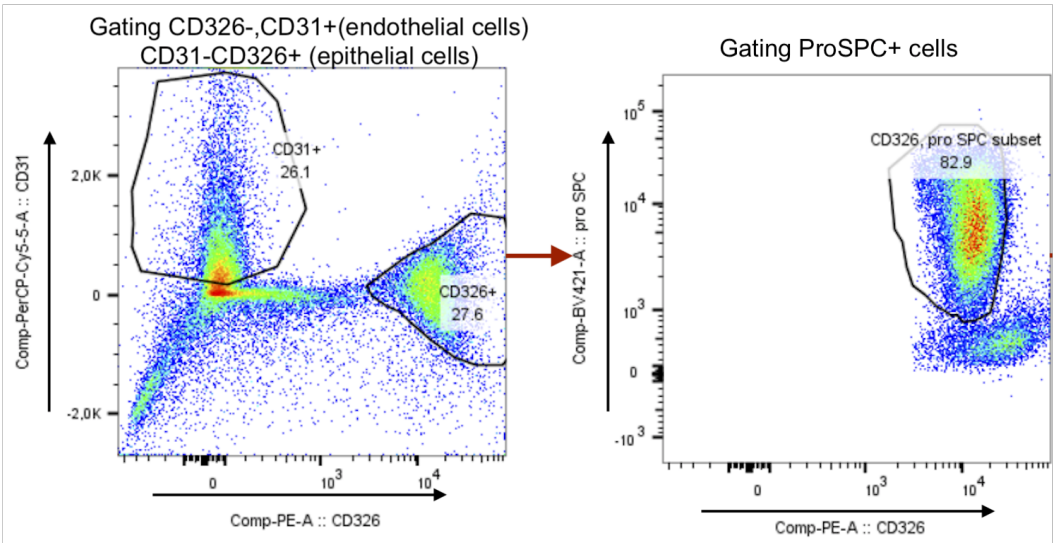

Figure 5.7: Gating strategy of the 8-color panel was the same as before until gating CD326+ from CD45- → ProSPC+ → living ProSPC+; CD326+ → living CD326+.

In the extended panel of staining, ProSPC marker worked well and the fraction of AT-II cells were higher in all of the protocols, that was in the range of 82-94% of total CD326+ cells for all the different protocols. High frequency ProSPC positive populations, which are AT-II cells, shows that the permeabilization worked well.

CD74, which is also a AT-II marker was found in a proportion of the dead cells that coexpressed ProSPC. This finding is similar to *Hasagawa et al 2017* [21] where very little of CD74 is found by surface staining. To generate higher CD74, staining intracellularly was needed. Similarly, no positive staining from T1a could be detected in the live epithelial population. The reason for this could be both that no AT-I cells were recovered or the fact that the antibody was incompatible with flow cytometry. Staining of the epithelial cells type should be repeated after an optimal lung dissociation protocol to yield the different epithelial cell types.

Mouse lung dissociation experiments showed a good progress from the beginning towards the final experiment in terms of both the single cell concentrations and the fraction of extracted cell types.
It was concluded from these experiments that treatment of the lungs with dispase inflation already at the time of tissue harvest in the very beginning results in higher yield of epithelial population. The total measured number of cells using counting beads was also significantly increased when using this method. Although the results are preliminary and more replicates are needed for solid conclusions, Protocol 3 combined with manual mincing had the highest epithelial cell recovery.

Table 5.1: Viability of key cell types listed for the different Protocols as the average of duplicates ± standard deviation (STD) in percentage.

Cell type	*in vivo* treatment	1: Dissociator	2: Dissociator	3: Dissociator	1:Manual mincing	2:Manual mincing	3:Manual mincing
Hematopoietic cells	Dispase	90,1±1,1	90,7±0,1	89,7±0,2	81,7±12,4	92,7±0,6	90,1±0,9
	N/A	86,7±2,5	89,6±0,9	90,1±0,4			
Endothelial cells	Dispase	86,5±3,7	95,3±1,3	92,1±0,9	75,6±4,6	90,2±0,2	69,8±1,2
	N/A	61,6±1,7	11,9±0,3	47,1±6,7			
Epithelial cells	Dispase	82,8±1,6	84,8±6,1	79,6±2,3	87,1±10,2	91,8±1,3	90,7±0,6
	N/A	82,5±3,8	67,2±9,1	76,6±2,6			
Non-lineage cells	Dispase	81,9±2,2	90,5±0,8	87,4±0,8	78,7±5,6	88,5±2,7	76,5±1,3
	N/A	87,7±5,3	69,7±1,9	87,7±1,3			

5.2 eGFP mRNA transfection in LA-4 cells

LA-4 cells were used to establish methods to measure mRNA protein translation after transfection with eGFP mRNA. The use of a fluorescent protein enabled real-time image analysis of the protein expression using Incucyte S3. The ambition was to develop a mouse *in vitro* system employing lung epithelial cells that could be used to monitor mRNA expression to differentiate between various LNPs prior to *in vivo* testing.
LA-4 cells were transfected with eGFP mRNA in two separate experiments. In the first experiment, a bacterial contamination was observed in some wells. Moreover, as the reagent was added as a small volume to the edge of each well in the first experiment, a so called edge-effect could be observed in the Incucyte S3 real time images, which is visualized in Figure 4.3. This resulted in an initial protein expression in the cells found at the edge of mRNA:Lipofectamine MessengerMAX delivery, which in turn affected the analysis metric when the measured data was normalized by the area of the well. In order to avoid this effect, the mRNA:Lipofectamine MessengerMax complex were mixed into the growth medium and then added to the wells at the same time as media exchange. This resulted in higher total eGFP signal as well as higher percentage of transfected cells.

5.2.1 Cell growth

The LA-4 cells were seeded in three different densities. The cell morphology is shown in Figure 5.8. LA-4 have irregular cytoplasmic projections when growing on plastic surfaces and become more rounded when intracellular contact is established. The cells are quite granular and stop proliferating when the culture reaches a confluent monolayer.[41]

The cell growth during eGFP expression in the 96-well plate was also measured along with the fluorescence signal. Representative curves for each cell density from the second experiment are presented in Figure 5.9. The time to maximum confluency depended on the start cell density, as expected. The cell growth was the same for all of the wells in both experiments, excluding the bacteria-contaminated wells from the first experiment. The idea of testing different cell densities was to examine the differences in transfection efficiency. The supplier of Lipofectamine MessengerMAX recommended a cell density close to 70-90% confluency at the time of transfection for effective transfection with less toxicity.

5.2.2 eGFP expression

eGFP protein expression was monitored over 72 hours for the different cell densities to investigate parameters such as total eGFP expression and percentage of eGFP-expressing cells over time for different doses of eGFP mRNA formulated in Lipofectamine MessengerMAX. The mRNA:Lipofectamine MessengerMax complexes were not removed from the media, so the accumulating fluorescence over time depended

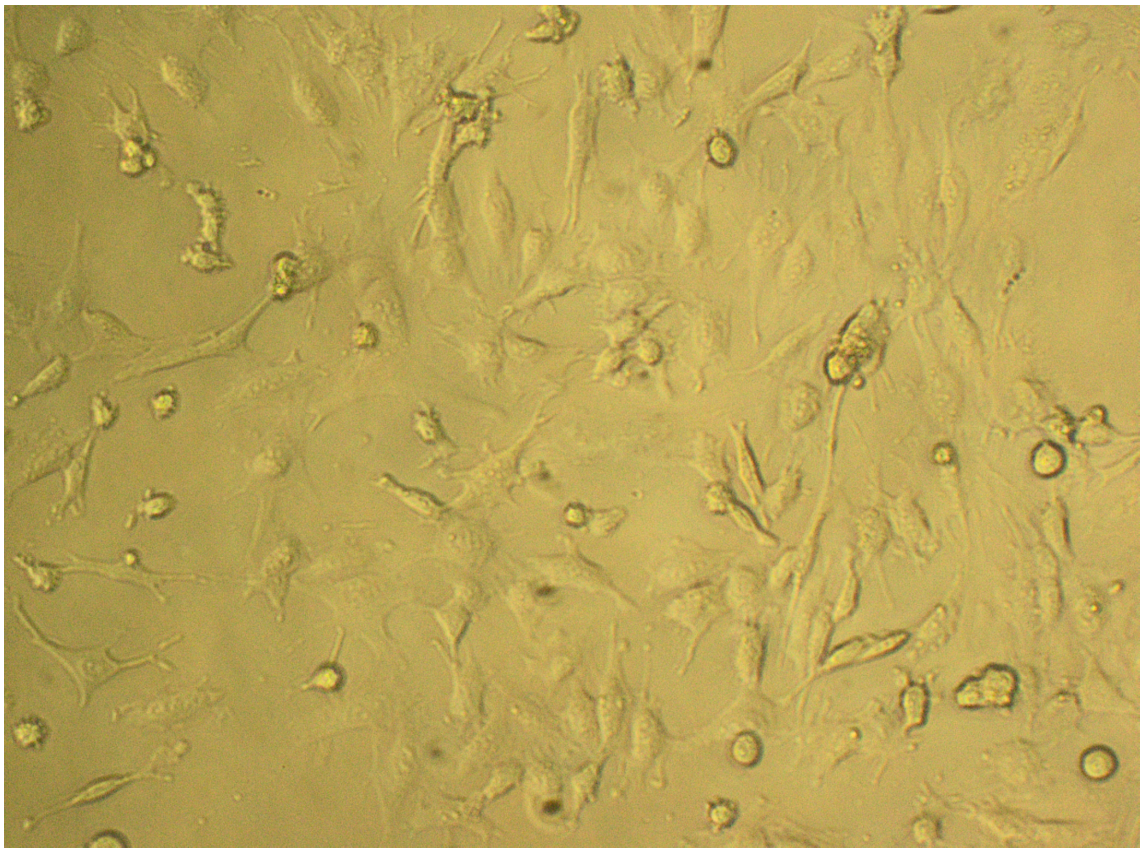

Figure 5.8: LA-4 cells grown in a well plate on the second day, settled on the bottom plate, 5000 cells/well in 10x magnification.

both on the continuous transfection and the stability of the eGFP protein.
Transfection of eGFP mRNA using Lipofectamine MessengerMax resulted in high expression of eGFP protein, starting already at 2h after transfection and increasing up to 18-24h where a plateau was reached. Figure 5.10 shows the total green object integrated intensity, i.e the total accumulated eGFP protein fluorescence over the first 24h for both experiments at mRNA dose of 250ng/cm^2. As can be seen from the two graphs, the fluorescence increased dramatically when the mRNA:Lipofectamine MessengerMAX complexes where mixed into the media (Experiment 2) and then added to the cells compared to when added in a smaller volume to the cells (Experiment 1). Both the experiments show that the maximum expression is reached at the same time for the maximum cell density, namely at 16-18 hours after the transfection. The fact that the LA-4 cells took up the mRNA segments and translated them effectively is very promising and Lipofectamine MessengerMAX could be used as a control reagent when investigating the protein expression obtained for different lipid nanoparticles in future.

In parallel to the Incucyte S3 eGFP measurements, 24h samples for flow cytometry measurements were also collected in the second experiment. eGFP expression reaches the maximum intensity at 16-24 hours depending on cell density and this is the reason for choosing dose-response of 24h for different mRNA doses. Gating

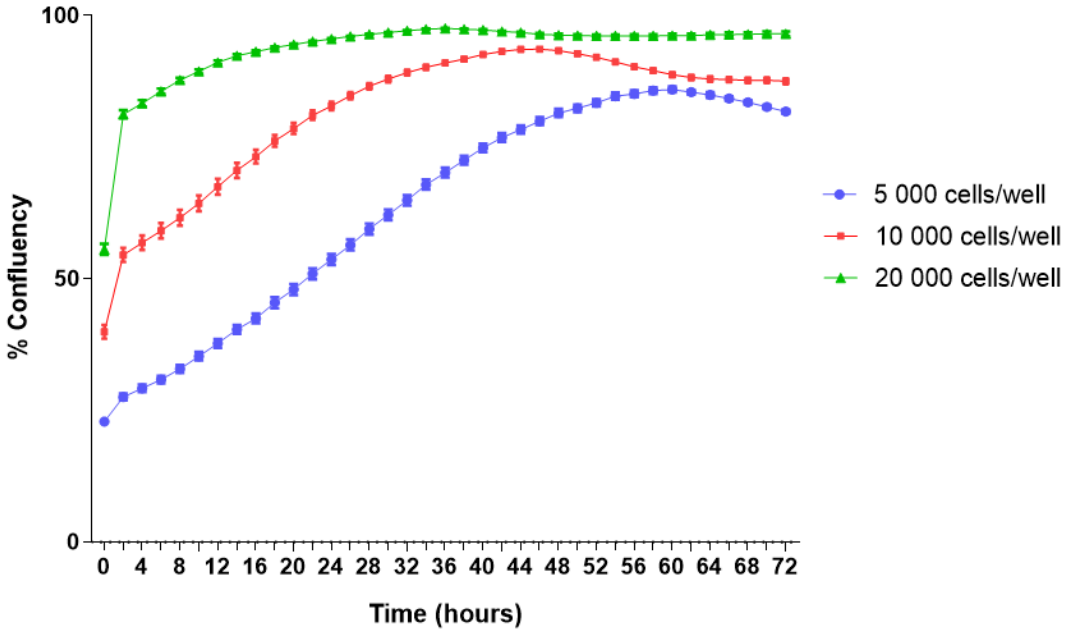

Figure 5.9: Mean growth rate of the cell cultures for three different cell densities are shown as Phase object confluence(%) for 72 hours transfection.

strategy of this experiment is found in Appendix A.2.1. Dose response in terms of fluorescence intensity and percentage of eGFP expressing cells were analyzed with the data Incucyte S3, and compared to flow cytometry results at 24h, which is presented in Figure 5.11. Still, the total integrated fluorescence intensity, calculated from IncuCyte S3, could not be compared directly with the flow cytometry analyzed fluorescence intensity, as the data from the Incucyte S3 measurements describe the total fluorescence whereas the flow cytometry measurements (MFI) gives a median of the eGFP fluorescence in the cell population. This is why the resulting MFI values are higher at lower cellular density compared to the total eGFP protein expressed that is highest for higher cell densities as presented by the Incucyte S3 data. The fraction of eGFP expressing cells analyzed from flow cytometry, on the other hand, can be compared to the metric green area/phase area of the real-time image analysis, as it gives the fraction of eGFP expressing cells per well.

To conclude, these experiments found that mixing the transfection reagent with the cell growth medium before adding it to the wells will increase eGFP protein expression. However, to more accurately determine the dynamics of protein translation following the transfection with mRNA, one need to do experiments where the mRNA:Lipofectamine MessengerMAX complexes are removed at fixed time-points by exchange of cell media. Here, the formulated mRNA was present for the entire course of the experiment, and the transfection might be a continuous process over longer time.

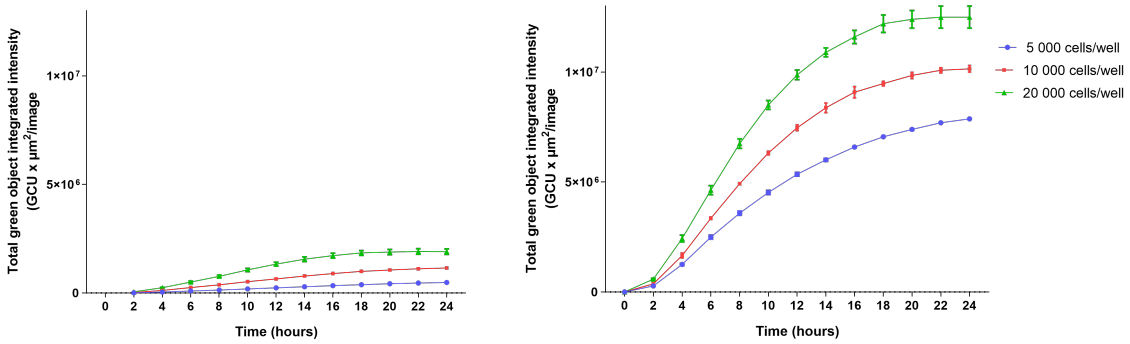

Figure 5.10: Total eGFP fluorescence signal is given as Total green object integrated intensity over 24 hours from transfection. The curves correspond to 3 different cell densities and mRNA dose of ng/cm^2. Left: result from experiment-1. (The first reading of the experiment started two hours later than the second experiment) Right: result from experiment-2.

5.3 eGFP mRNA transfection in human lung tissue

In order to measure the protein translation after mRNA transfection in human lung tissue, an initial experiment on lung tissue explants transfected with eGFP mRNA:Lipofectamine MessengerMax similar to that of LA-4 cells. The transfection experiment was conducted over 24h and the explants were then harvested and homogenized for measurements of resulting eGFP protein expression using an eGFP ELISA kit. The obtained eGFP protein was then normalised against total protein in all tissue lysates using the BCA protein assay. The transfection of 1-3 pieces per well was investigated and the resulting data is shown in Figure 5.12
The results from eGFP mRNA transfection of human lung explants shows that it is possible to achieve mRNA transfection and protein translation also in tissue pieces. Next steps would be to optimize the transfection conditions and investigate which lung cells take up and express the eGFP protein, by dissociation of the lung pieces into single cell suspension and cell characterization by flow cytometry. Although in its initial state, this method might have the potential to increase the understanding of the mode of action of different LNPs that can assist in the drug development preclinically as well as investigating the translation between human and rodents. Despite promising initial data, the method requires further optimization and development of characterizing flow cytometry panels to elucidate cell-specific expression.

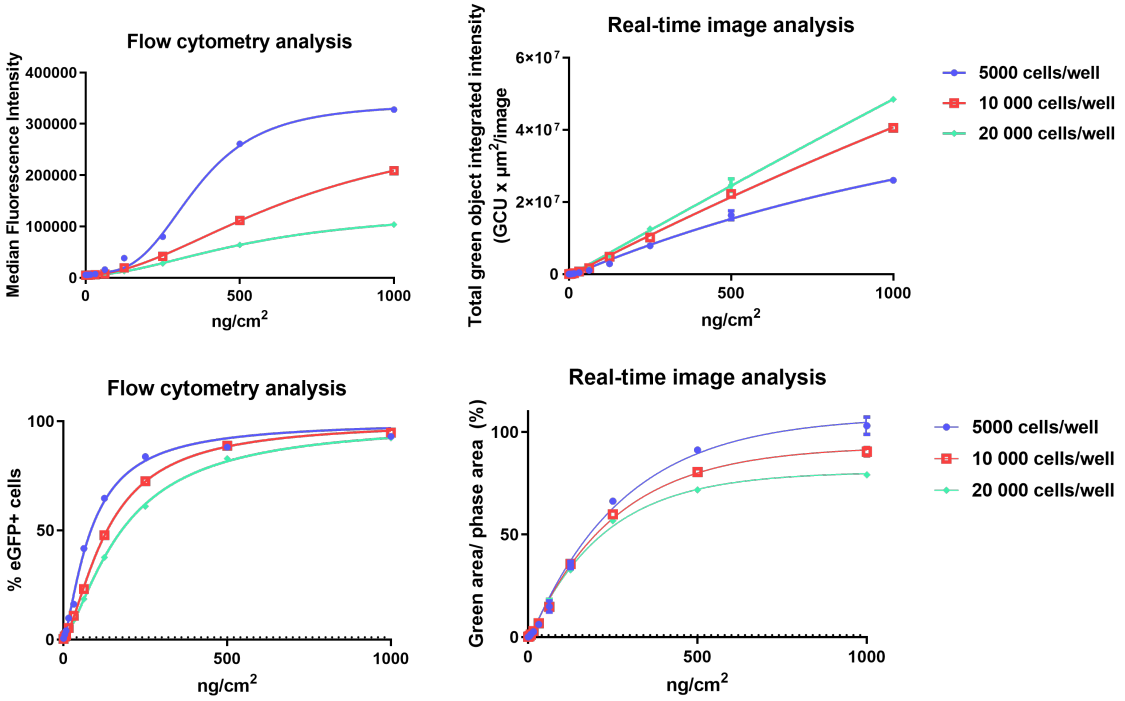

Figure 5.11: Dose response analysis of data generated from real-time image analysis and flow cytometry analysis at 24h post-transfection of eGFP mRNA. Top left: Median fluorescence intensity calculated from analyzing the flow cytometry data. Top right: Total integrated intensity analyzed from the real-time images. Bottom left: Fraction of eGFP expressing cells analyzed from flow cytometry. Bottom right: Green area/phase area in percentage, analyzed from the real-time images.

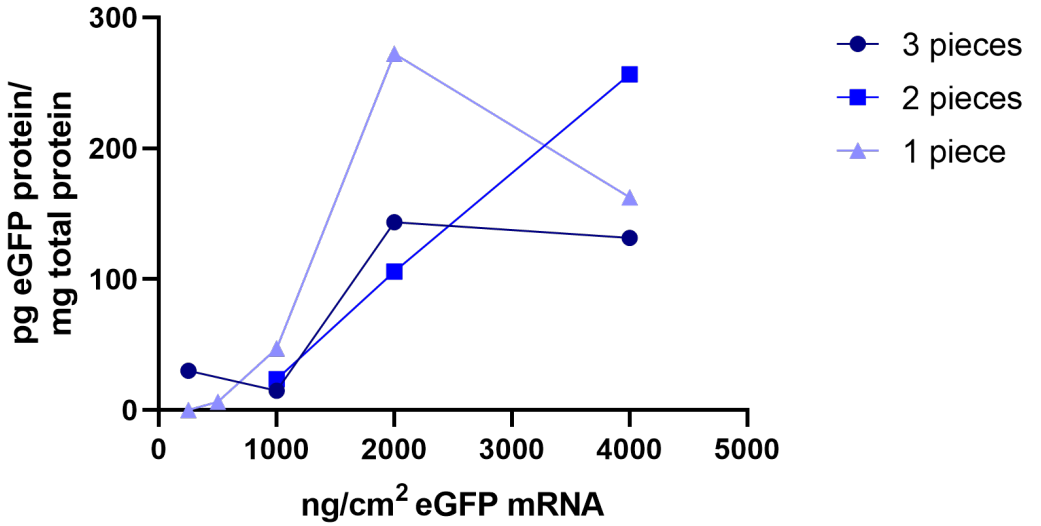

Figure 5.12: Dose response analysis of eGFP protein amount in picogram (pg) normalized by the total protein amount in milligram (mg) against eGFP mRNA:Lipofectamine reagent dosages in ng/cm^2 at 24j post-transfection.

6
Conclusion and perspectives

mRNA therapeutics holds a broad potential in future treatment of a wide range of diseases, including lung diseases. In this thesis, the focus was to develop methods to measure downstream protein expression following mRNA treatment. We have shown the great advantage of dispase inflation of the lung *in vivo* combined with consecutive enzymatic and mechanical *in vitro* dissociation when it comes to optimizing the recovery of lung epithelial cells. However, optimization of protocols and more replicates are still needed prior to selection of an optimal dissociation protocol. Development of new flow cytometry panels to further characterize the different types of epithelial cells recovered in the dissociation methods is also critical for optimal selection of dissociation method. Furthermore, flow cytometry sorting could be used for extraction of specific epithelial lung cell populations that could be cultivated and transfected with mRNA:LNP *in vitro*. In this way, mouse lung dissociation and cell sorting could assist in the validation and selection of mRNA:LNP formulation both from *in vivo* and *in vitro* experiments.

The second part of this thesis involved *in vitro* experiments investigating the dynamics of protein translation after eGFP mRNA:Lipofectamine MessengerMax transfection in a mouse lung epithelial cell line (LA-4). This method enables monitoring of protein expression live in future validation experiments of different LNP formulations to maximize uptake and translation of the mRNA.
The initial experiment towards development of a translational method for measuring mRNA protein translation in human lung explants was successful. Although a lot more development and validation of this method is needed, eGFP expression was achieved after eGFP mRNA:Lipofectamine MessengerMax transfection. *Ex vivo* experiments using human bronchial tissue explants in conjunction with cell characterization by flow cytometry and measures of translated protein could possibly explain an often seen lack of translation between *in vivo* and *in vitro* (cell culture) experiments. This method also offers the possibility to test the mRNA:LNP formulations on human lung tissue preclinically.

Bibliography

[1] C. P. Page and P. J. Barnes, *Pharmacology and Therapeutics of Asthma and COPD*. Springer, Cham, 2017, vol. 237.

[2] U. Demkow and F. J. Van Overveld, "Role of elastases in the pathogenesis of chronic obstructive pulmonary disease: Implications for treatment," *European Journal of Medical Research*, vol. 15, no. 2, pp. 27–35, 11 2010.

[3] V. D. Rose, K. Molloy, S. Gohy, C. Pilette, and C. M. Greene, "Airway Epithelium Dysfunction in Cystic Fibrosis and COPD," *Mediators of Inflammation*, vol. 2018, 2018.

[4] "World Health Organization(WHO), Chronic obstructive pulmonary disease (COPD)." [Online]. Available: https://www.who.int/news-room/fact-sheets/detail/chronic-obstructive-pulmonary-disease-(copd)

[5] "Global Initiative for Chronic Obstructive Lung Disease - GOLD." [Online]. Available: https://goldcopd.org/about-us/

[6] J. Yhee, J. Im, and R. Nho, "Advanced Therapeutic Strategies for Chronic Lung Disease Using Nanoparticle-Based Drug Delivery," *Journal of Clinical Medicine*, vol. 5, no. 9, p. 82, 9 2016.

[7] P. J. Barnes, P. G. Burney, E. K. Silverman, B. R. Celli, J. Vestbo, J. A. Wedzicha, and E. F. Wouters, "Chronic obstructive pulmonary disease," *Nature Reviews Disease Primers*, vol. 1, 12 2015.

[8] P. S. Kowalski, A. Rudra, L. Miao, and D. G. Anderson, "Delivering the Messenger: Advances in Technologies for Therapeutic mRNA Delivery," vol. 27, no. 4, pp. 710–728, 4 2019.

[9] U. Sahin, K. Karikó, and Türeci, "MRNA-based therapeutics-developing a new class of drugs," *Nature Reviews Drug Discovery*, vol. 13, no. 10, pp. 759–780, 1

2014.

[10] M. A. Islam, E. K. Reesor, Y. Xu, H. R. Zope, B. R. Zetter, and J. Shi, "Biomaterials for mRNA delivery," *Biomaterials Science*, vol. 3, no. 12, pp. 1519–1533, 12 2015.

[11] J. L. Kirschman, S. Bhosle, D. Vanover, E. L. Blanchard, K. H. Loomis, C. Zurla, K. Murray, B. C. Lam, and P. J. Santangelo, "Characterizing exogenous mRNA delivery, trafficking, cytoplasmic release and RNA-protein correlations at the level of single cells," *Nucleic Acids Research*, vol. 45, no. 12, 7 2017.

[12] "Study to Evaluate the Safety Tolerability of MRT5005 Administered by Nebulization in Adults With Cystic Fibrosis (RESTORE-CF)." [Online]. Available: https://clinicaltrials.gov/ct2/show/NCT03375047

[13] "Safety and Immunogenicity Study of 2019-nCoV Vaccine (mRNA-1273) for Prophylaxis of SARS-CoV-2 Infection (COVID-19)." [Online]. Available: https://clinicaltrials.gov/ct2/show/NCT04283461

[14] B. Connolly, C. Isaacs, L. Cheng, K. H. Asrani, and R. R. Subramanian, "SERPINA1 mRNA as a Treatment for Alpha-1 Antitrypsin Deficiency," *Journal of Nucleic Acids*, vol. 2018, 2018.

[15] "AstraZeneca and MedImmune enter strategic collaboration with Ethris to develop mRNA therapies for respiratory diseases." [Online]. Available: https://www.astrazeneca.com/media-centre/articles/2017/astrazeneca-and-medimmune-enter-strategic-collaboration-with-ethris-to-develop-mrna-therapies-for-respirator-diseases-17082017.html

[16] "Lipofectamine MessengerMAX | Thermo Fisher Scientific - SE." [Online]. Available: https://www.thermofisher.com/se/en/home/brands/product-brand/lipofectamine/lipofectamine-messengermax.html

[17] S. S. Negus and M. L. Banks, "Pharmacokinetic–Pharmacodynamic (PKPD) Analysis with Drug Discrimination," in *Current Topics in Behavioral Neurosciences*. Springer Verlag, 2018, vol. 39, pp. 245–259.

[18] G. J. Tortora, *Introduction to the human body : the essentials of anatomy and physiology*, 10th ed. Hoboken, N.J. Wiley, cop. 2015, 2015.

[19] " Cells of Origin for Lung Cancer - Comparative Dosimetry of Radon in Mines and Homes - NCBI Bookshelf," Tech. Rep., 1991.

[20] A. El-Hashash and A. El-Hashash, *Brief Overview of the Human Respiratory System Structure and Development*. Springer International Publishing, 2018.

[21] K. Hasegawa, A. Sato, K. Tanimura, K. Uemasu, Y. Hamakawa, Y. Fuseya, S. Sato, S. Muro, and T. Hirai, "Fraction of MHCII and EpCAM expression characterizes distal lung epithelial cells for alveolar type 2 cell isolation," *Respiratory Research*, vol. 18, no. 1, 8 2017.

[22] M. C. Williams, "Alveolar Type I Cells: Molecular Phenotype and Development," *Annual Review of Physiology*, vol. 65, no. 1, pp. 669–695, 3 2003.

[23] K. Kawabata, T. Hagio, and S. Matsuoka, "The role of neutrophil elastase in acute lung injury," pp. 1–10, 9 2002.

[24] L. M. Salazar and A. M. Herrera, "Fibrotic Response of Tissue Remodeling in COPD," 2011.

[25] K. R. Bracke and G. G. Brusselle, "Chronic Obstructive Pulmonary Disease," in *Mucosal Immunology: Fourth Edition*. Elsevier Inc., 4 2015, vol. 2-2, pp. 1857–1866.

[26] M. Aghapour, P. Raee, S. J. Moghaddam, P. S. Hiemstra, and I. H. Heijink, "Airway Epithelial Barrier Dysfunction in Chronic Obstructive Pulmonary Disease: Role of Cigarette Smoke Exposure," *American Journal of Respiratory Cell and Molecular Biology*, vol. 58, no. 2, pp. 157–169, 2018.

[27] N. Sanders, C. Rudolph, K. Braeckmans, S. C. De Smedt, and J. Demeester, "Extracellular barriers in respiratory gene therapy," *Advanced Drug Delivery Reviews*, vol. 61, no. 2, pp. 115–127, 2 2009.

[28] W. Filipowicz, Y. Furuichi, J. M. Sierra, S. Muthukrishnan, A. J. Shatkin, and S. Ochoa Roche, "A protein binding the methylated 5'-terminal sequence, m7GpppN, of eukaryotic messenger RNA (Artemia salina embryos/cap binding protein)," Proc. Natl. Acad. Sci. USA, Tech. Rep. 5, 1976.

[29] S. Vaidyanathan, K. T. Azizian, A. K. Haque, J. M. Henderson, A. Hendel, S. Shore, J. S. Antony, R. I. Hogrefe, M. S. Kormann, M. H. Porteus, and A. P. McCaffrey, "Uridine Depletion and Chemical Modification Increase

Cas9 mRNA Activity and Reduce Immunogenicity without HPLC Purification," *Molecular Therapy - Nucleic Acids*, vol. 12, pp. 530–542, 9 2018.

[30] M. Maugeri, M. Nawaz, A. Papadimitriou, A. Angerfors, A. Camponeschi, M. Na, M. Hölttä, P. Skantze, S. Johansson, M. Sundqvist, J. Lindquist, T. Kjellman, I. L. Mårtensson, T. Jin, P. Sunnerhagen, S. Östman, L. Lindfors, and H. Valadi, "Linkage between endosomal escape of LNP-mRNA and loading into EVs for transport to other cells," *Nature Communications*, vol. 10, no. 1, pp. 1–15, 12 2019.

[31] J. C. Kaczmarek, P. S. Kowalski, and D. G. Anderson, "Advances in the delivery of RNA therapeutics: From concept to clinical reality," *Genome Medicine*, vol. 9, no. 1, 6 2017.

[32] K. S. Stenn, R. Link, G. Moellmann, J. Madri, and E. Kuklinska, "Dispase, a Neutral Protease From Bacillus Polymyxa, is a Powerful Fibronectinase and Type IV Collagenase," *Journal of Investigative Dermatology*, vol. 93, no. 2, pp. 287–290, 8 1989.

[33] "Collagenase - Worthington Enzyme Manual." [Online]. Available: http://www.worthington-biochem.com/cls/default.html

[34] "DNase I." [Online]. Available: https://www.thermofisher.com/order/catalog/product/18047019#/18047019

[35] T. Bushnell, "Modern Flow Cytometry," Expert Cytometry LLC, Tech. Rep., 2015.

[36] M. Roederer, "Spectral compensation for flow cytometry: Visualization artifacts, limitations, and caveats," *Cytometry*, vol. 45, no. 3, pp. 194–205, 11 2001.

[37] "Flow Cytometry - A Survey and the Basics." [Online]. Available: https://www.labome.com/method/Flow-Cytometry-A-Survey-and-the-Basics.html

[38] "FlowJo | FlowJo, LLC." [Online]. Available: https://www.flowjo.com/solutions/flowjo

[39] "CountBright Absolute Counting Beads." [Online]. Available: https://www.thermofisher.com/document-connect/document-connect.html?url=https%3A%2F%2Fassets.thermofisher.com%

2FTFS-Assets%2FLSG%2Fmanuals%2Fmp36950.pdf&title=
Q291bnRCcmlnaHQgQWJzb2x1dGUgQ291bnRpbmcgQmVhZHM=

[40] "Incucyte® S3 Live-Cell Analysis System." [Online]. Available: https://www.essenbioscience.com/en/products/incucyte/incucyte-s3/

[41] G. D. Stoner, Y. Kikkawa, A. J. Kniazeff, K. Miyai, and R. M. Wagner, "Clonal Isolation of Epithelial Cells from Mouse Lung Adenoma | Cancer Research," *cancer research 35*, pp. 2177–2185, 8 1975.

[42] G. Zhang, V. Gurtu, and S. R. Kain, "An enhanced green fluorescent protein allows sensitive detection of gene transfer in mammalian cells," *Biochemical and Biophysical Research Communications*, vol. 227, no. 3, pp. 707–711, 10 1996.

[43] "GraphPad Prism 8." [Online]. Available: https://www.graphpad.com/scientific-software/prism/

[44] "The Anatomy of the Laboratory Mouse." [Online]. Available: http://www.informatics.jax.org/cookbook/figures/figure53.shtml

[45] "Sysmex XP-300™ Automated Hematology Analyzer." [Online]. Available: https://www.sysmex.com/us/en/Products/Hematology/3PartDiff/Pages/XP-300-Hematology-Analyzer.aspx

[46] "LA-4 (ATCC® CCL-196™)." [Online]. Available: https://www.atcc.org/Products/All/CCL-196.aspx

[47] "Lung dissociation kit - Miltenyi Biotec ," 2017. [Online]. Available: https://www.miltenyibiotec.com/_Resources/Persistent/0b0d3e21e2e0de71053c528b8bd293e3a2289ac5/DS_Lung%20Dissociation%20Kit_m.pdf

[48] B. D. Singer, J. R. Mock, F. R. D'alessio, N. R. Aggarwal, P. Mandke, L. Johnston, and M. Damarla, "Flow-cytometric method for simultaneous analysis of mouse lung epithelial, endothelial, and hematopoietic lineage cells," *Am J Physiol Lung Cell Mol Physiol*, vol. 310, pp. 796–801, 2016.

A

Appendix

A.1 Mouse lung dissociation

A.1.1 Protocol of initial lung dissociation

i. Prepare 6 GentleMACS C tubes (two for each enzyme mixture) and prepare 2.5 mL of the enzyme mix following the corresponding boxes.

ii. Receive tissues in PBS on ice. Divide up two lung lobes (right and lower left) into 2 C tubes with prepared enzyme mixtures 1, 2 and 3 (total of 6 samples).

1.

1X Buffer S	2.4 mL
Solution D	100 µL
Solution A	15 µL

2.

Collagenase/Dispase (1mg/mL)	25 µL
DNAse I (100U/mL)	1.34 µL
PBS	2475 µL

3.

Dispase II(2.4U/mL)	67 µL
Collagenase III (150U/mL)	218 µL
DNAse I (100U/mL)	1.34 µL
PBS	2214 µL

iii. Mince the lung lobes into small pieces and rinse them with PBS before transferring them into the tubes with 1.25 mL of enzyme mixture.

iv. Close the lids completely, place the tubes into GentleMACS^{TM} Octo dissociator with heaters on and run GentleMACS^{TM} Octo dissociator program *37C_m_LDK_1*.

v. Filter the sample through 100 µm cell strainer with pipettes and transfer to a 50 mL tube.

vi. Wash C tube with 5 mL FACS buffer and mix carefully, then pour the solution to the 50 mL tube.

vii. Centrifuge the samples in 350g for 10 minutes and aspirate supernatant.

viii. Resuspend the pellet in 0.5 mL 1x of ACK Lysis buffer and Incubate at room temperature for 3-5 minutes.

ix. Resuspend the pellet in 2 mL of FACS buffer and filter the samples again through a 100 µM cell strainer prior to proceed to the staining.

A.1.2 Protocol of dispase method lung dissociation

- Anesthetize the mouse by intraperitoneal injection of pentobarbital (200 mg/mL, 0.2 mL mouse).
- Perfuse PBS via heart (right ventricle, 27G needle, 10 mL ice cold PBS) with an incision made in the left atrium for drainage.
- Via tracheal cannula, inflate lung with RT dispase solution (∼2 mL), tie off trachea to retain dispase inside lung, harvest the inflated lung, and place in ice cold PBS.

i. Prepare 6 GentleMACS C tubes (two for each enzyme mixture) for the dissociator protocols and prepare 6 petri-dishes for manual mincing protocols.

ii. Prepare ∼12 mL of the enzyme mix following the corresponding boxes.

ii. Receive tissues in PBS on ice. Divide up into lung lobes (right and other left lobes) into 2 C tubes and 2 petri-dishes with prepared enzyme mixtures 1, 2 and 3 (total of 6 samples).

1.		
	1X Buffer S	11.448 mL
	Solution D	480 µL
	Solution A	72 µL

2.		
	Collagenase/Dispase(1mg/mL)	240 µL
	DNAse I (100U/mL)	1.64 µL
	PBS	1200 µL

3.		
	Dispase II(2.4 U/mL)	3200 µL
	Collagenase III (150 U/mL)	1047 µL
	DNAse I (100 U/mL)	1.60 µL
	PBS	7753 µL

iii. Mince the lung lobes into small pieces and rinse them with PBS before transferring them into the petri-dishes with ∼3 mL of enzyme mixture.

iv. Incubate the tissues in the enzyme mix for 40-45minutes in 37 °C with occasional agitaion.

v. After 30min, add 1.64 µL of DNAse to Protocol 2 Dishes, add 1.60 µL of DNAse to Protocol 3 Dishes and put back in 37 °C incubator for 10min.

vi. Filter through 100 µM cell strainer with pipettes and transfer to a 50 ml tube. Rinse the Dishes with 5 mL PBS to get back all the cells.

iii. Close lids of the tubes completely and place into GentleMACS^{TM} Octo dissociator. No heaters and run GentleMACS^{TM} Octo dissociator program *m_impTumor_02* (6x tubes).

iv. Incubate the tubes for 40-45minutes in 37 °C with occasional agitaion.

v. After 30min, add 1.64uL of DNAse to Protocol 2 tubes, add 1.60uL of DNAse to Protocol 3 tubes and put back in 37 °C incubator for 10min.

vi. Run GentleMACS^{TM} Octo dissociator program *m_impTumor_03*, filter through 100 µM cell strainer with pipettes and transfer to a 50 ml tube. Rinse the dishes with 6 mL PBS to get back all the cells.

vii. Centrifuge the samples in 310g for 5 minutes and aspirate the supernatant.

viii. Resuspend the pellet in 2 mL 1x of ACK Lysis buffer and Incubate at RT for 3-5 minutes.

ix. Resuspend pellet in 2 mL FACS buffer, filter the samples again through a 100 µm cell strainer and proceed to the staining.

A.1.3 FMO controls used in 4-color staining panels

Table A.1: Volumes in µL of antibodies prepared for the FMO controls used in the final experiment of dispase method.

Component	**FMO-Live/Dead**	**FMO-CD45**	**FMO-CD31**	**FMO-CD326**
FITC Rat anti-mouse CD45	0,50	0	0,50	0,50
APC Rat ani-mouse CD326	1	1	1	0
PE Rat Anti-mouse CD31	1	1	0	1
Purified rat anti-mouse CD16/CD32 (FC block)	1	1	1	1
Fixable viability dye eFluor ^{TM} 780 (Live/dead)	0	0,1	0,1	0,1
FITC Rat IgG2b, κ Isotype Control	0	0,50	0	0
APC Rat IgG2a, κ isotype Control	0	0	0	1
PE Rat IgG2a, κ isotype Control	0	0	1	0
FACS buffer	97,50	97,50	97,50	97,50
Total volume (µL)	**100**	**100**	**100**	**100**

A.1.4 Results from 8-color staining panel

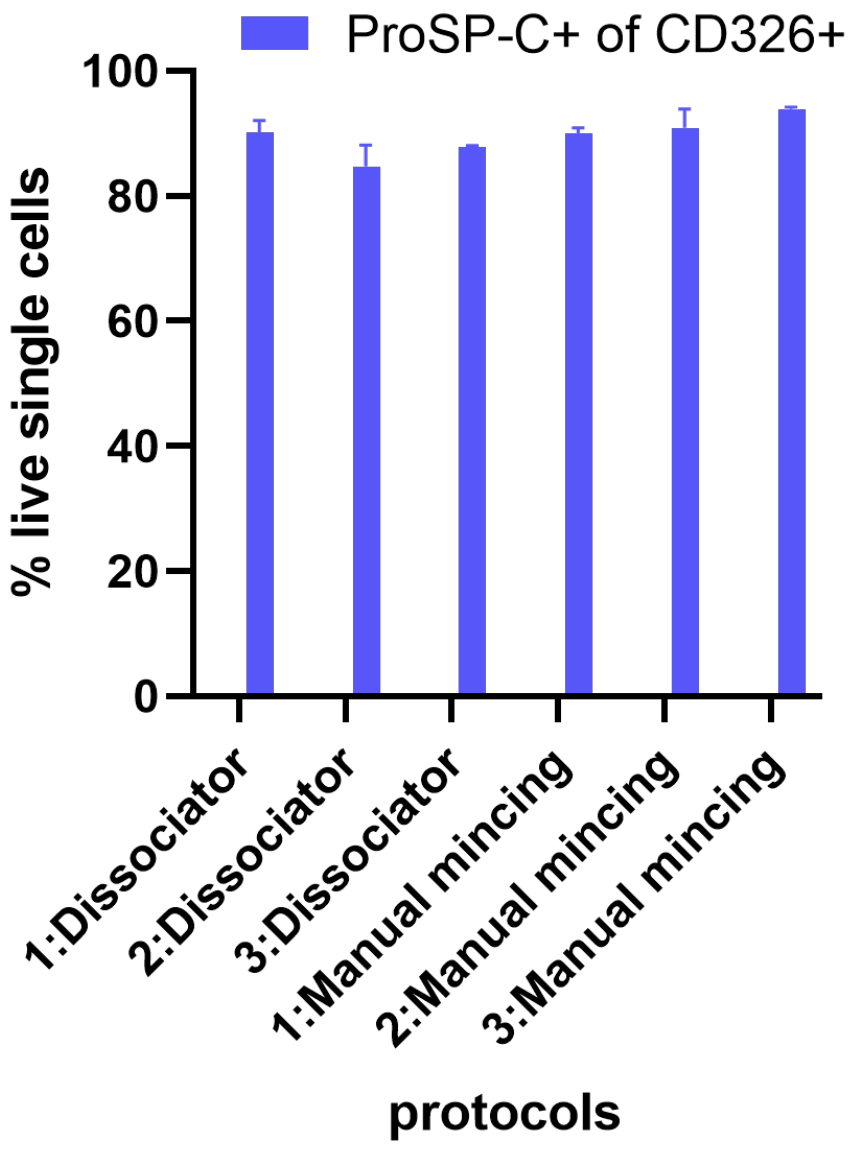

Figure A.1: Frequency of live single population of ProSP-C+ cells (AT-II) which was calculated based on the total epithelial cells from 8-color staining panel.

A.1.5 Cell count of the final lung dissociation experiment of dispase method comparing the manual measurements using Sysmex hematometer

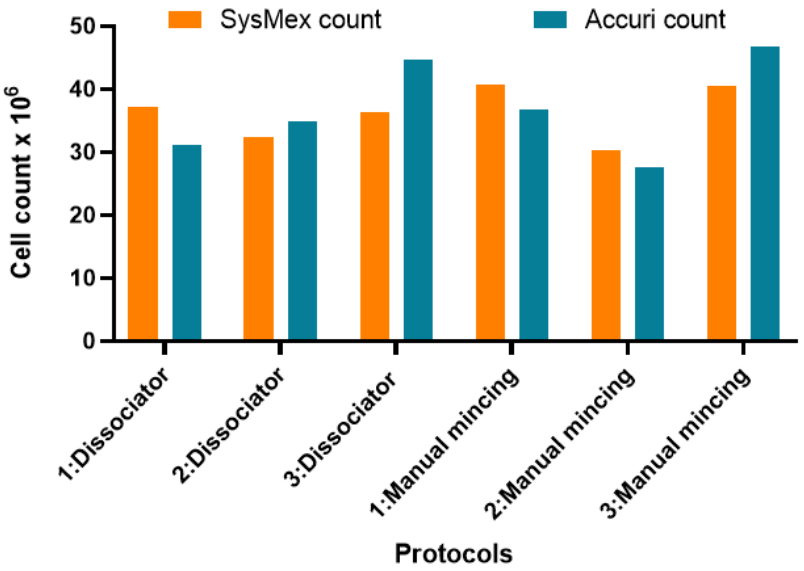

Figure A.2: Total cell count (left and right lobes) in millions, cell count on flow cytometry and on hematometer.

A.2 eGFP mRNA transfection

A.2.1 Gating strategy of eGFP expression analysis in flow cytometry

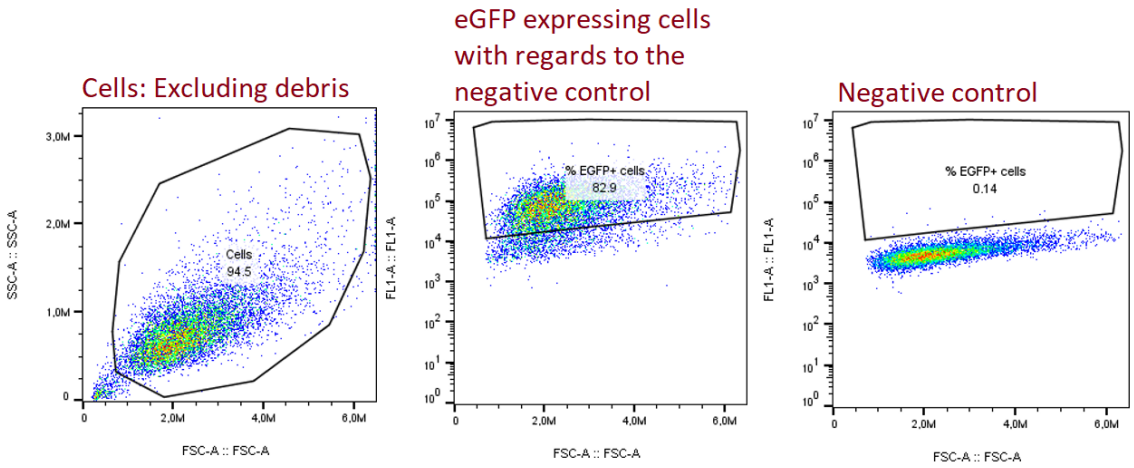

Figure A.3: eGFP protein expression analysis in LA-4 cells by flow cytometry. Cells were gated excluding the debris. eGFP expressing expressing cells were gated visualizing the "cells" population against corresponding flow cytometry filter, which is FL1 in this case. The gate of eGFP+ expression was set considering the negative (untransfected) control. Median fluorescence intensity was calculated by extracting the median of each cell populations. The fraction of eGFP expressing cells were calculated by extracting the corresponding frequency of parent populations and then subtracting eGFP cells from the whole cell population.